

Homeostatic Cytokines Drive Epigenetic Reprogramming of Activated T Cells into a "Naive-Memory" Phenotype

Frumento, Guido; Verma, Kriti; Croft, Wayne; White, Andrea; Zuo, Jianmin; Nagy, Zsuzsanna; Kissane, Stephen; Anderson, Graham; Moss, Paul; Chen, Frederick E

DOI:

[10.1016/j.isci.2020.100989](https://doi.org/10.1016/j.isci.2020.100989)

License:

Creative Commons: Attribution (CC BY)

Document Version

Publisher's PDF, also known as Version of record

Citation for published version (Harvard):

Frumento, G, Verma, K, Croft, W, White, A, Zuo, J, Nagy, Z, Kissane, S, Anderson, G, Moss, P & Chen, FE 2020, 'Homeostatic Cytokines Drive Epigenetic Reprogramming of Activated T Cells into a "Naive-Memory" Phenotype', *iScience*, vol. 23, no. 4, 100989. <https://doi.org/10.1016/j.isci.2020.100989>

[Link to publication on Research at Birmingham portal](#)

General rights

Unless a licence is specified above, all rights (including copyright and moral rights) in this document are retained by the authors and/or the copyright holders. The express permission of the copyright holder must be obtained for any use of this material other than for purposes permitted by law.

- Users may freely distribute the URL that is used to identify this publication.
- Users may download and/or print one copy of the publication from the University of Birmingham research portal for the purpose of private study or non-commercial research.
- User may use extracts from the document in line with the concept of 'fair dealing' under the Copyright, Designs and Patents Act 1988 (?)
- Users may not further distribute the material nor use it for the purposes of commercial gain.

Where a licence is displayed above, please note the terms and conditions of the licence govern your use of this document.

When citing, please reference the published version.

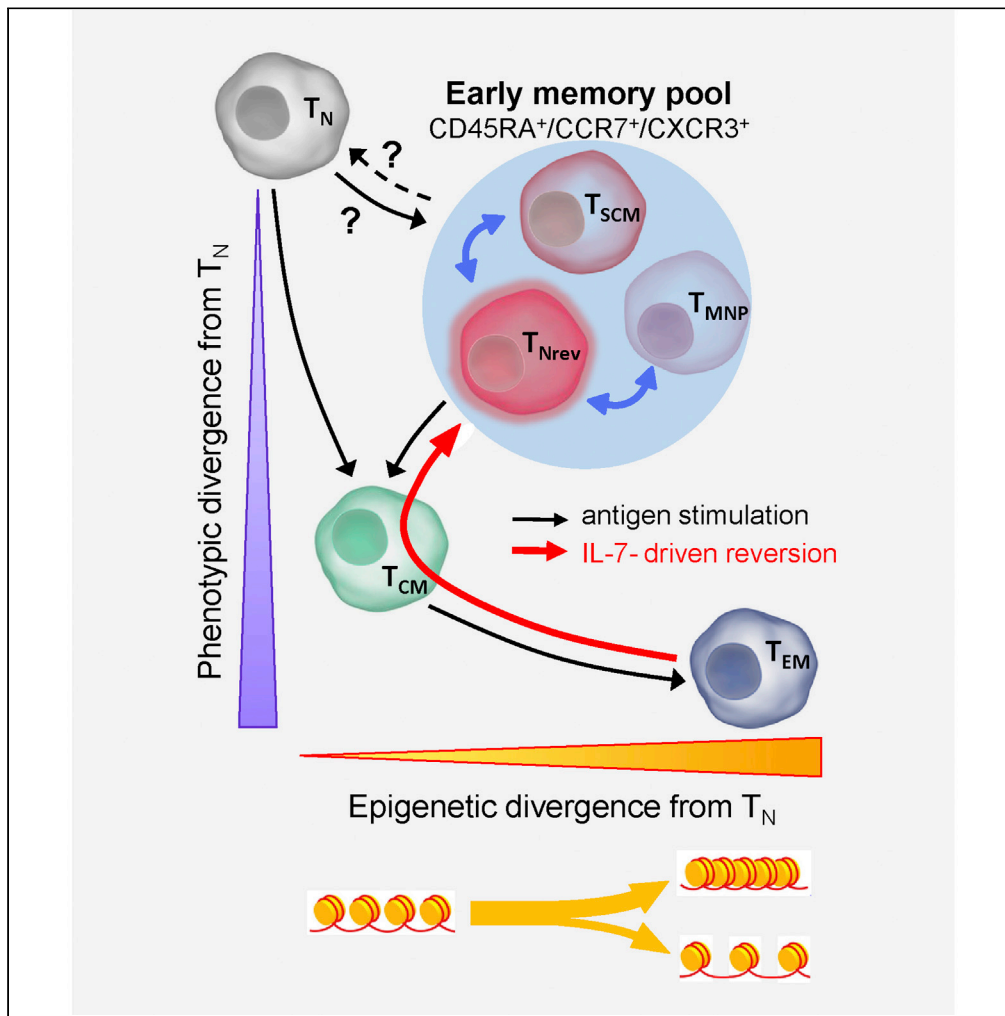
Take down policy

While the University of Birmingham exercises care and attention in making items available there are rare occasions when an item has been uploaded in error or has been deemed to be commercially or otherwise sensitive.

If you believe that this is the case for this document, please contact UBIRA@lists.bham.ac.uk providing details and we will remove access to the work immediately and investigate.

Article

Homeostatic Cytokines Drive Epigenetic Reprogramming of Activated T Cells into a “Naive-Memory” Phenotype



Guido Frumento,
Kriti Verma,
Wayne Croft, ...,
Graham
Anderson, Paul
Moss, Frederick E.
Chen

p.moss@bham.ac.uk (P.M.)
frederick.chen@nhs.net
(F.E.C.)

HIGHLIGHTS

γ -chain cytokines revert newly differentiated CD8⁺ T cells to a naive-like phenotype

These “naive-revertant” are primed for secondary challenge

Their chromatin landscape is reminiscent of memory cells

Specific signaling pathways and transcription factors are involved

DATA AND CODE

AVAILABILITY

GSE114812

Frumento et al., iScience 23, 100989
April 24, 2020 © 2020 The Author(s).
<https://doi.org/10.1016/j.isci.2020.100989>



Article

Homeostatic Cytokines Drive Epigenetic Reprogramming of Activated T Cells into a “Naive-Memory” Phenotype

Guido Frumento,^{1,2} Kriti Verma,^{1,9} Wayne Croft,^{1,3,9} Andrea White,¹ Jianmin Zuo,¹ Zsuzsanna Nagy,⁴ Stephen Kissane,⁵ Graham Anderson,¹ Paul Moss,^{1,6,10,11,*} and Frederick E. Chen^{1,2,7,8,10,*}

SUMMARY

Primary stimulation of T cells is believed to trigger unidirectional differentiation from naive to effector and memory subsets. Here we demonstrate that IL-7 can drive the phenotypic reversion of recently differentiated human central and effector memory CD8⁺ T cells into a naive-like phenotype.

These “naive-revertant” cells display a phenotype similar to that of previously reported stem cell memory populations and undergo rapid differentiation and functional response following secondary challenge. The chromatin landscape of reverted cells undergoes substantial epigenetic reorganization with increased accessibility for cytokine-induced mediators such as STAT and closure of BATF-dependent sites that drive terminal differentiation. Phenotypic reversion may at least partly explain the generation of “stem cell memory” CD8⁺ T cells and reveals cells within the phenotypically naive CD8⁺ T cell pool that are epigenetically primed for secondary stimulation. This information provides insight into mechanisms that support maintenance of T cell memory and may guide therapeutic manipulation of T cell differentiation.

INTRODUCTION

The development of T cell memory is essential for long-term health but it remains uncertain how this population is maintained over the many decades of human lifespan. Current models of CD8⁺ T cell differentiation propose a unidirectional and irreversible pathway whereby initial antigen stimulation triggers sequential differentiation of naive (T_N) cells into central memory (T_{CM}), effector memory (T_{EM}), and effector (T_{EF}) T cells (Klebanoff et al., 2006). T cells gradually acquire increasing effector function but this is associated with a progressive reduction in the capacity for differentiation and self-renewal, i.e., “stemness.” In settings of persistent antigenic stimulations T cells may progressively lose effector functions and proliferative capacity such that they eventually become exhausted.

Two subsets of phenotypically naive CD8⁺ T cells with features of memory cells have recently been described. “T-memory stem cells” (T_{SCM}), which display enhanced capacity for self-renewal and multipotent proliferative potential (Gattinoni et al., 2011), are believed to be minimally differentiated and located between T_N and T_{CM} in the differentiation pathway (Gattinoni et al., 2017). “Memory T cells with naive phenotype” (T_{MNP}) also exhibit broad polyfunctional capability (Pulko et al., 2016) and are thought to be functionally imprinted at an early stage of differentiation between CD8⁺ T_N and T_{CM} subsets. Despite sharing many characteristics, T_{SCM} and T_{MNP} differ in their extended phenotype and it is uncertain if they represent distinct and stable subsets or derive from a common precursor with phenotypic plasticity. Although CD8⁺ T_{SCM} can be produced *in vitro* by activating T_N cells in the presence of interleukin (IL)-7, IL-21, and the glycogen synthase-3β inhibitor TWS119 (Sabatino et al., 2016), the physiological mechanisms leading to the generation of both these cells and T_{MNP} are largely unknown.

Given the importance of cytokines as key regulators of T cell-mediated immunity, we analyzed the effect of different cytokines on T cell differentiation after primary stimulation, using T cells from human cord blood (CB), which are unlikely to have encountered antigen and therefore have a very low frequency of T_{SCM} (Gattinoni et al., 2011). We observed that recently differentiated CD8⁺ memory T cells can undergo lineage reversion to a naive-like phenotype when exposed to γ-chain cytokines and that these naive-revertant cells

¹Institute of Immunology and Immunotherapy, University of Birmingham, Birmingham, UK

²NHS Blood and Transplant, Birmingham, UK

³Centre for Computational Biology, University of Birmingham, Birmingham, UK

⁴Institute of Inflammation and Ageing, University of Birmingham, Birmingham, UK

⁵Technology Hub, University of Birmingham, Birmingham, UK

⁶Centre for Clinical Haematology, University Hospitals Birmingham NHS Foundation Trust, Birmingham, UK

⁷Clinical Haematology, Barts Health NHS Trust, London, UK

⁸Blizard Institute, Queen Mary University London, London, UK

⁹These authors contributed equally

¹⁰These authors contributed equally

¹¹Lead Contact

*Correspondence: p.moss@bham.ac.uk (P.M.), frederick.chen@nhs.uk (F.E.C.)

<https://doi.org/10.1016/j.isci.2020.100989>



share extensive phenotypic and functional characteristics with both T_{SCM} and T_{MNP} . This work describes a new pathway of T cell differentiation and provides a unifying theory for the generation of T cells with a “naive-memory” profile.

RESULTS

IL-7 Induces Recently Differentiated $CD8^+$ Memory T Cells to Revert to a Naive-like Phenotype

CB mononuclear cells (CBMCs) were activated with anti-CD3 plus IL-2, and the differentiation stage of $CD8^+$ T cells was evaluated by CD45RA and CCR7 co-expression (Klebanoff et al., 2006). As expected, activation induced an expansion of T_{CM} ($CD45RA^-/CCR7^+$) and T_{EM} ($CD45RA^-/CCR7^-$) subsets with a concurrent reduction in T_N ($CD45RA^+/CCR7^+$) (Figures 1A and 1B). T_{Eff} ($CD45RA^+/CCR7^-$) were not generated in significant number and were not considered further.

In order to investigate the role of cytokines in determining the fate of recently differentiated memory $CD8^+$ T cells, IL-7 was added to the culture medium when the proportion of $CD8^+$ T_N dropped below 20% of the $CD8^+$ population, typically around 1 week after activation (6.7 ± 1.9 days, mean \pm 1 SD, $n = 50$). No further activation stimulation was given. In the first 3 days following addition of IL-7 the percentage of $CD8^+$ T_N continued to diminish, reaching a nadir of $8.4\% \pm 6.40$ (Figure 1B). However, with continuing IL-7 incubation the great majority of $CD8^+$ T cells started to re-express CD45RA and reverted back to a phenotype resembling T_N and characterized by co-expression of CD45RA, CCR7, CD62L, and CD27 and loss of CD45RO expression (Figures 1A and S1A). We termed these cells that reverted to a naive-like phenotype as “T naive-revertant” (T_{Nrev}). This re-acquisition of a naive-like phenotype by $CD8^+$ memory T cells reached a plateau by 13–28 days after initial activation (20 ± 4.7 days) and typically represented over 70% of the $CD8^+$ T cell population (mean $71\% \pm 12$, range 45%–95%). As such, this value was only slightly below the mean of 87% of $CD8^+$ T_N at day 0 (± 5.8 , range 74–98). All samples followed a similar pattern, although there was variation both in the time taken to reach the peak T_{Nrev} level and in the magnitude of the T_{Nrev} population at plateau (Figure 1B). These differences in the percentage of cells with naive phenotype between day 0 and nadir, and between nadir and plateau, were highly significant ($p = 1.99 \times 10^{-50}$ and $p = 2.69 \times 10^{-38}$, respectively, by paired t test).

To demonstrate that the phenotypic reversion of differentiated T cells was not due to selective death or proliferation of individual T cell subsets, we enumerated the cells within each cell subset and monitored their proliferation. The total number of all cell subsets before and after reversion remained largely unchanged (Table S1), and no cell proliferation was detected after the addition of IL-7 and during the period of phenotypic reversion (Figure 1C). To further confirm that the phenomenon was due to modulation of cellular phenotype, recently differentiated $CD8^+$ T_{CM} and T_{EM} were purified, incubated with IL-7, and tracked. Phenotypic reversion was again demonstrated for over 80% of the purified T_{CM} and T_{EM} (Figure 1D).

T_{Nrev} May Undergo Several Rounds of Differentiation and Reversion

We next assessed whether this property was unique to IL-7 or shared by other cytokines. Recently differentiated CBMCs were incubated with single and multiple combinations of the γ -chain cytokines IL-2, IL-7, IL-15, IL-4, and IL-21. IL-6, an inflammatory cytokine, was also incorporated.

Phenotypic reversion was observed with several of these cytokines, but IL-7 was the most potent agent (Figure 1E). Interestingly, $CD8^+$ T cells cultured with IL-6 or IL-21 were driven toward a more differentiated phenotype with a substantial increase in T_{Eff} cells. No synergistic effect was observed when IL-7 was administered together with IL-2, IL-4, or IL-15. In addition, the ability of individual cytokines to promote dedifferentiation to T_{Nrev} cells was correlated with their ability to maintain $CD8^+$ T cell survival *in vitro* (Figure 1F), whereas IL-6, IL-21, or medium alone led to substantial cell death. This suggests that reversion may be a default physiological program of recently differentiated $CD8^+$ T cells when a survival stimulus is provided.

Phenotypic reversion also takes place following differentiation induced by mitogenic stimuli other than soluble anti-CD3 (Figure 1G). The percentage of differentiated $CD8^+$ T cells undergoing IL-7-dependent phenotype reversion after activation with phytohemagglutinin (PHA) and staphylococcus enterotoxin B (SEB) was similar to those following activation with anti-CD3. Activation with CD3/CD28 beads led to a smaller proportion of differentiated cells reverting to a naive phenotype, but we were unable to fully

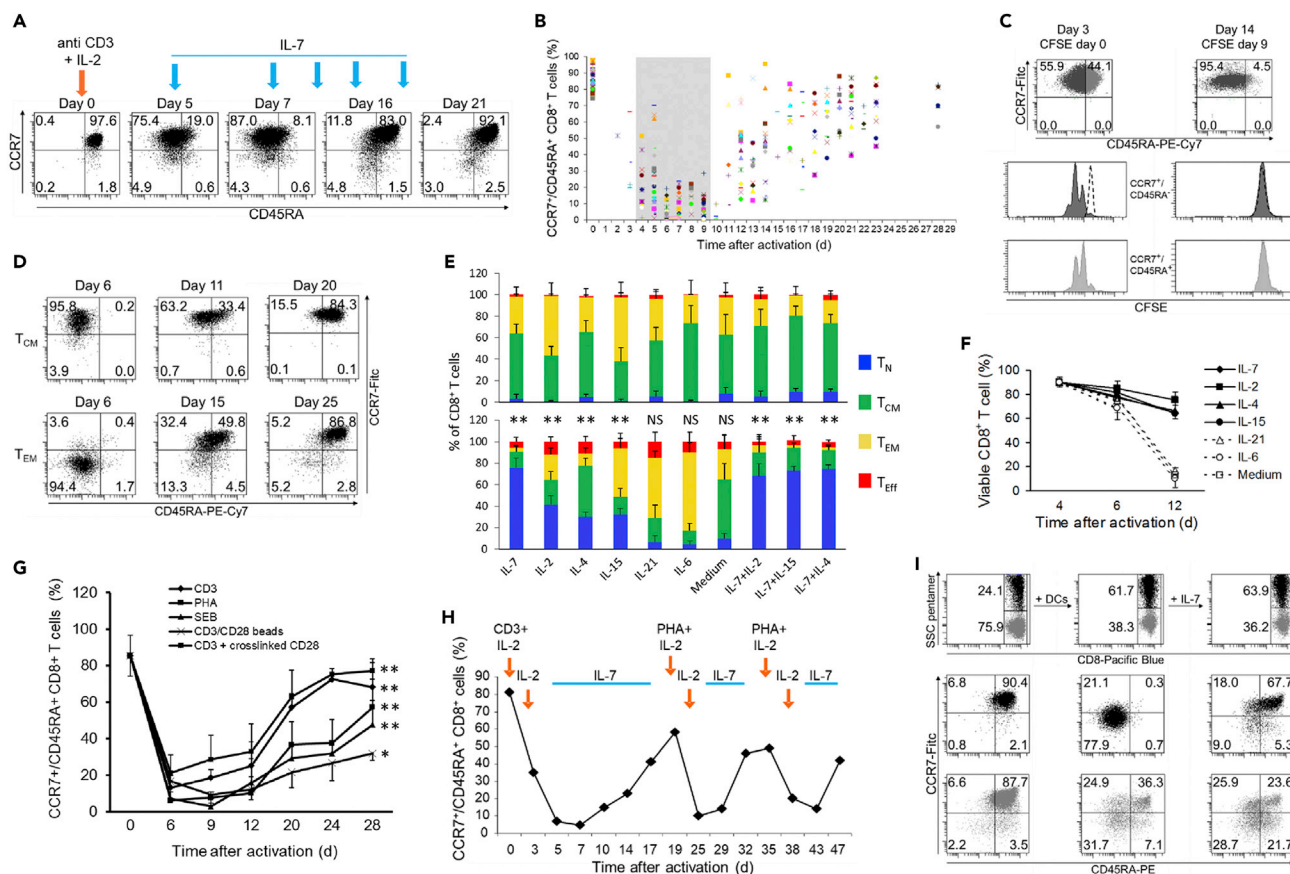


Figure 1. IL-7 Induces Reversion of Recently Differentiated Memory CD8⁺ T Cells to a Naive-like Phenotype

(A) Flow cytometric analysis of phenotypic changes in CD8⁺ T cells after activation and successive incubation with 25 ng/mL IL-7. CBMCs were activated with anti-CD3 plus IL-2, and when the percentage of CD8⁺ T_N dropped below 20%, in this case day 5, cultures were maintained in IL-7. Numbers indicate the percentage of cells in each quadrant. Single representative experiment out of 50.

(B) Kinetics of phenotype reversion of CD8⁺ T cells from the 50 different CB samples. Each symbol represents one sample. The shaded area indicates the interval of time when IL-7 was added for the first time.

(C) CD8⁺ T cell proliferation after activation and IL-7 administration. CBMCs were stained with CFSE either before activation (left panels) or at day 9, during phenotype reversion (right panels). At the indicated time points, cell phenotype and CFSE content were assessed for T_N (light gray dots) and T_{CM} (dark gray dots). Dashed lines indicate basal content in CFSE. Single representative experiment out of three.

(D) Flow cytometry evaluation of IL-7-dependent phenotype reversion in recently differentiated T_{CM} and T_{EM}. After activation T_{CM} and T_{EM} were negatively selected. The two cell subpopulations were then incubated with IL-7 and monitored for phenotype changes over time. Single representative experiment out of three, for each subset.

(E) The effect of different cytokines on phenotype reversion. CBMCs were activated, and when the percentage of CD8⁺ T_N dropped below 20% the indicated cytokines were added. The percentage of the cells in the different subsets is shown when the percentage of CD8⁺ T_N reached the nadir (upper panel) and afterward, when it reached the plateau (lower panel). Data from six samples. Paired t test analysis between the T_N levels at nadir and plateau. ** = p < 0.001.

(F) Viability of cells incubated with different cytokines. Activated CBMCs were incubated from day 4 with each cytokine or medium, and CD8⁺ T cell viability was evaluated by flow cytometry using 7-AAD uptake. Data are represented as means ± 1SD of three samples.

(G) The kinetics of phenotype reversion of CD8⁺ T cells activated with different artificial stimuli. Data are represented as means ± 1SD of three samples. Paired t test analysis between the T_N levels at nadir and plateau. * = p < 0.05, ** = p < 0.001.

(H) The kinetics of phenotype reversion of CD8⁺ T cells undergoing successive cycles of activation/IL-7 incubation. Newly generated CD8⁺ T_{Nrev} cells were twice re-stimulated with PHA and induced to revert twice with IL-7 when the percentage of T_N dropped below 20%. Single representative experiment out of three.

(I) Flow cytometry analysis of phenotype changes of CD8⁺ T_{Nrev} upon activation with the cognate antigen. CB T lymphocytes were activated, retrovirally transduced with the SSC-TCR, and induced to revert their phenotype with IL-7 (left panels). Afterward, cells were incubated with peptide-pulsed DCs (central panels). IL-7 was then added again, driving the transduced cells to revert their phenotype (right panels). Plots were gated on CD8⁺ T cells. The upper panels show the percentage of transduced (black dots) and non-transduced (gray dots) CD8⁺ T cells.

remove the beads, some of which were still attached to the cells when IL-7 was added, and it is likely that the resulting continuous antigen stimulation explains the lesser reversion achieved. However, the kinetics of reversion were similar demonstrating that co-stimulation does not prevent phenotypic reversion.

We further assessed whether cells could undergo more than one cycle of phenotypic reversion. Since serial rounds of anti-CD3 stimulation led to a high rate of cell death, PHA was used for two further rounds of activation, each followed by IL-7 incubation (Figure 1H). Phenotypic reversion was observed after each cycle of activation and IL-7 treatment, indicating that CD8⁺ T_N can undergo repeated cycles of differentiation and reversion.

In order to demonstrate that phenotypic reversion is also possible after activation with cognate antigen, CBMCs were transduced with a gene encoding a T cell receptor (TCR) specific for a peptide from the Epstein-Barr virus (EBV) LMP2 protein (Frumento et al., 2013). Following activation and retroviral transduction, cells acquired a predominantly T_{CM}/T_{EM} phenotype but reverted to T_{Nrev} when incubated with IL-7. Cells were then re-challenged with peptide-pulsed autologous dendritic cells (DCs) and underwent differentiation again to CD8⁺ T_{EM} within 5 days (Figure 1I). At this point IL-7 was re-added, and after a further 9 days a second reversion to T_{Nrev} was attained, demonstrating that phenotypic reversion is also possible after stimulation with cognate antigen presented by professional antigen-presenting cells.

CD8⁺ T_{Nrev} Proliferate and Differentiate Rapidly into Functional Effector Cells following Secondary Stimulation

As T_{Nrev} are antigen-experienced cells that have previously undergone differentiation and expansion we were interested to assess their proliferative potential when compared with primary T_N. After re-stimulation T_{Nrev} differentiated into memory subsets more rapidly than T_N and exhibited a higher proliferation rate (Figures 2A and 2B). T_{Nrev} also rapidly acquired effector function, and when EBV-specific TCR-transduced T_{Nrev} were re-stimulated with peptide-pulsed DCs and driven to a T_{EM} phenotype the cells expressed perforin and granzyme B (Figure 2C) and exerted cytolytic activity against target cells (Figure 2D).

T Cells from Cord Blood and Adult Donors Differ in Degree of Reversion and Chromatin Accessibility

In order to demonstrate that phenotypic reversion phenomenon is not just restricted to T cells from CB we next enriched CD8⁺ and CD4⁺ T_N cells from the blood of adult donors and compared their ability to revert to T_{Nrev} following *in vitro* activation (Figure 2E). Although the vast majority of CB-derived CD8⁺ T cells could be induced to revert to T_{Nrev}, this was seen in less than half of naive CD8⁺ T cells from peripheral blood (PB) of adult donors. The reduced degree of reversion in PB cells could not be related to differences in basal phenotype as these were identical in T_N cells from CB and PB (Figure S1B). Instead, a remarkable difference was found in the chromatin landscape of T_N from the two sources (Figure 2F), which is predicted to influence a range of biological processes (Figure S2A). Compared with T_N from PB, T_N from CB showed increased accessibility to sites binding transcription factors (TFs), in particular those from the basic region/leucine zipper motif (bZIP) family, of which BATF was the one with the highest number of open binding sites (Figure 2G). Moreover, T_{Nrev} showed more open chromatin regions annotated as regulatory sites for genes involved in TCR signaling (Figure S2B).

Only recently differentiated T_{CM} and T_{EM} were able to undergo reversion and not established T_{CM} (CCR7⁺/CD45RA⁻) and T_{EM} (CCR7⁻/CD45RA⁻) CD8⁺ T cells from adult blood (Figure 2H). This indicates that, despite similar phenotype, the capacity for IL-7-induced dedifferentiation is observed only within recently differentiated T_{CM} and T_{EM} and is relatively less efficient in adult donors.

T_{Nrev} Phenotype Overlaps with T_{SCM} and T_{MNP} during *In Vitro* Culture

Using available data (Christensen et al., 2001; Hendriks et al., 2003; Hermiston et al., 2003; Ishida et al., 1992; Kim et al., 2006; O'Shea et al., 1992; Zehnder et al., 1992) we identified 28 membrane-bound proteins that exhibit a differential pattern of expression following T cell activation and differentiation. Antibodies against these proteins were then used to contrast the phenotypic profile of T_N and T_{Nrev}. The pattern of expression of integrin β7, CD25, CD127, CD95, CXCR3, and CD49d was found to discriminate between these two subsets (Figure 3A). Interestingly, CD95 and CXCR3 are also distinct markers of T_{SCM} (Gattinoni et al., 2011) and CD49d is a marker of T_{MNP} (Pulko et al., 2016). T_{Nrev} and T_{CM} are clearly distinguished by CCR7 and CD45RA expression, but additional differences were also found in the expression of CD25, CD45RO, CD69, CD95, CD120b, CD122, and PTK7 (Figures 3A and S3). These differences demonstrate that the phenotypic correlates of reversion extend substantially beyond differential expression of CCR7 and CD45RA.

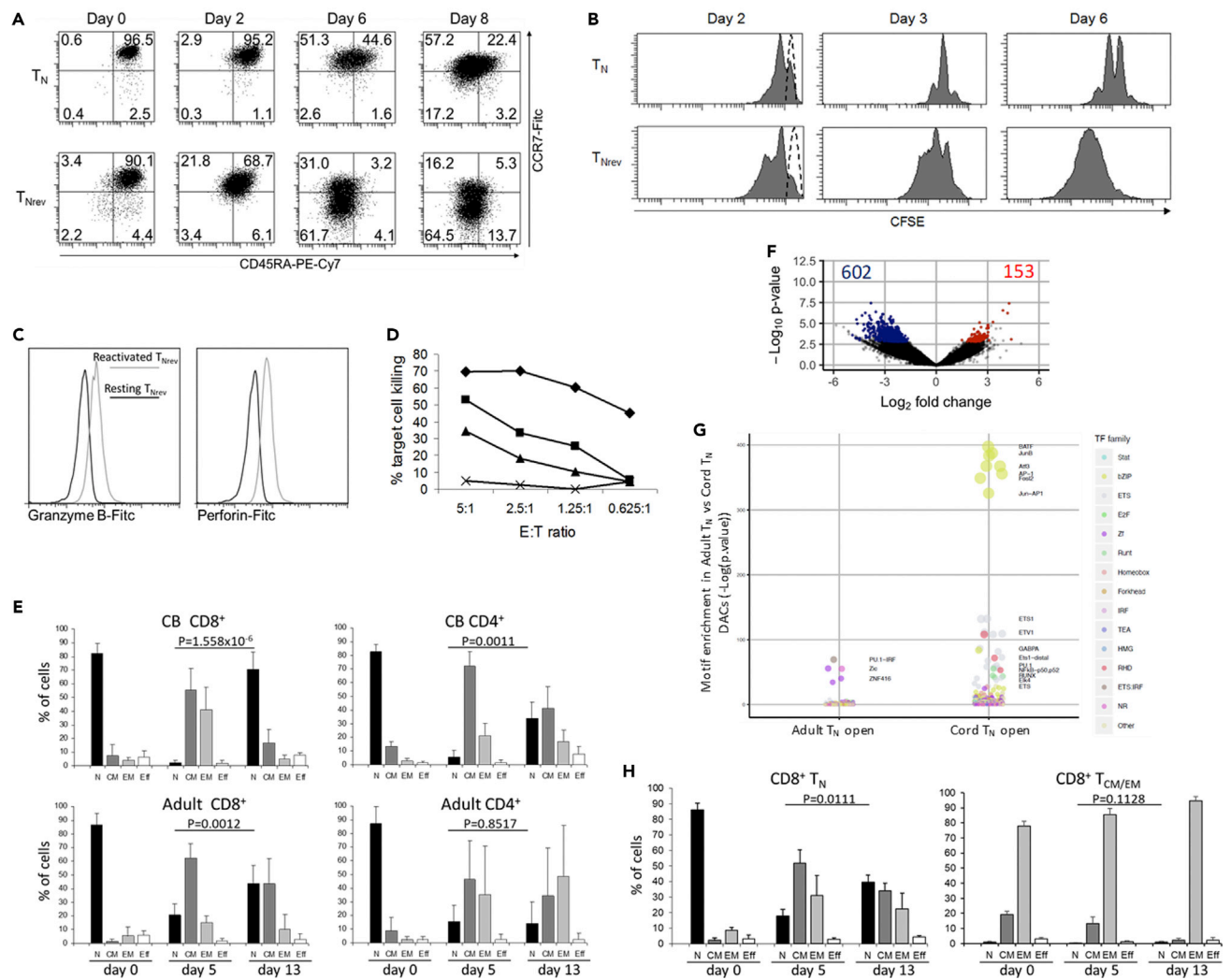


Figure 2. CD8⁺ T_{Nrev} Cells Have Excellent Differentiation and Proliferative Potential and the Amplitude of Reversion Depends on the Cell Source

(A) Flow cytometry analysis of phenotype changes in CD8⁺ T_{Nrev} and T_N cells from the same CB sample following stimulation with PHA. Single representative experiment out of three.

(B) Flow cytometry analysis of the proliferation of CD8⁺ T_{Nrev} and T_N cells. Cells from the samples shown in the panel above were stained with CFSE at day 0 and activated with PHA. The CFSE content in the two cell subsets is shown at the indicated time points. Dashed lines represent basal content of CFSE. Single representative experiment out of three.

(C) Flow cytometry analysis of perforin and granzyme B expression by the re-stimulated TCR-transduced CD8⁺ T_{Nrev}. The intracellular expression of perforin and granzyme B were assessed in T_{Nrev} cells transduced with the SSC-TCR after re-stimulating the cells twice with cognate peptide-pulsed DCs.

(D) Cytotoxic assay of re-stimulated, SSC-specific TCR-transduced T_{Nrev}. The T cells were incubated in a standard ⁵¹Cr cytolytic assay with target cells consisting of HLA A*1101-transduced T2 cells loaded with either 1 μg/mL (diamonds), 10 ng/mL (squares) or 1 ng/mL (triangles) of SSC peptide. The peptide solvent, i.e., DMSO, was used as control (crosses). The percentage of target cell killing at different E:T ratios is indicated.

(E) T_N cells were isolated from CBMCs and PBMCs, activated with PHA, and then incubated with IL-7. The percentage of cells in the different subsets was measured by flow cytometry at the indicated time points. Data are represented as mean ± 1SD of five CB samples and eight PB samples. Analysis by paired t test.

(F) Differential accessibility of peak regions identified in PB T_N cells versus CB T_N cells. The x axis indicates Log₂ fold change, and the y axis indicates -Log₁₀ p value of all peaks. Colored points indicate differentially accessible chromatin sites with inaccessible sites as blue and accessible sites as red. Data are from three CB and three PB samples.

(G) TF-binding motif enrichments at DACs more accessible in T_N from PB and from CB. Significant (FDR<0.1) pathway enrichments identified within DEG lists from T_{Nrev}.

(H) CD8⁺ T_N, T_{CM} and T_{EM}, were isolated from adult PB, activated with PHA, and incubated with IL-7 from day 5. The percentage of cells in the different subsets was measured by flow cytometry at the indicated time points. Data are represented as mean ± 1SD of three samples. Paired t test.

We next went on to investigate the relationship between T_{Nrev} cells and T_{SCM} and T_{MNP} subsets. In particular we were interested in the stability of the T_{Nrev} phenotype and how this could be modulated by culture conditions. CD8⁺ T_{Nrev} cells had a very similar phenotype to T_{SCM} and T_{MNP}, and all three expressed a common

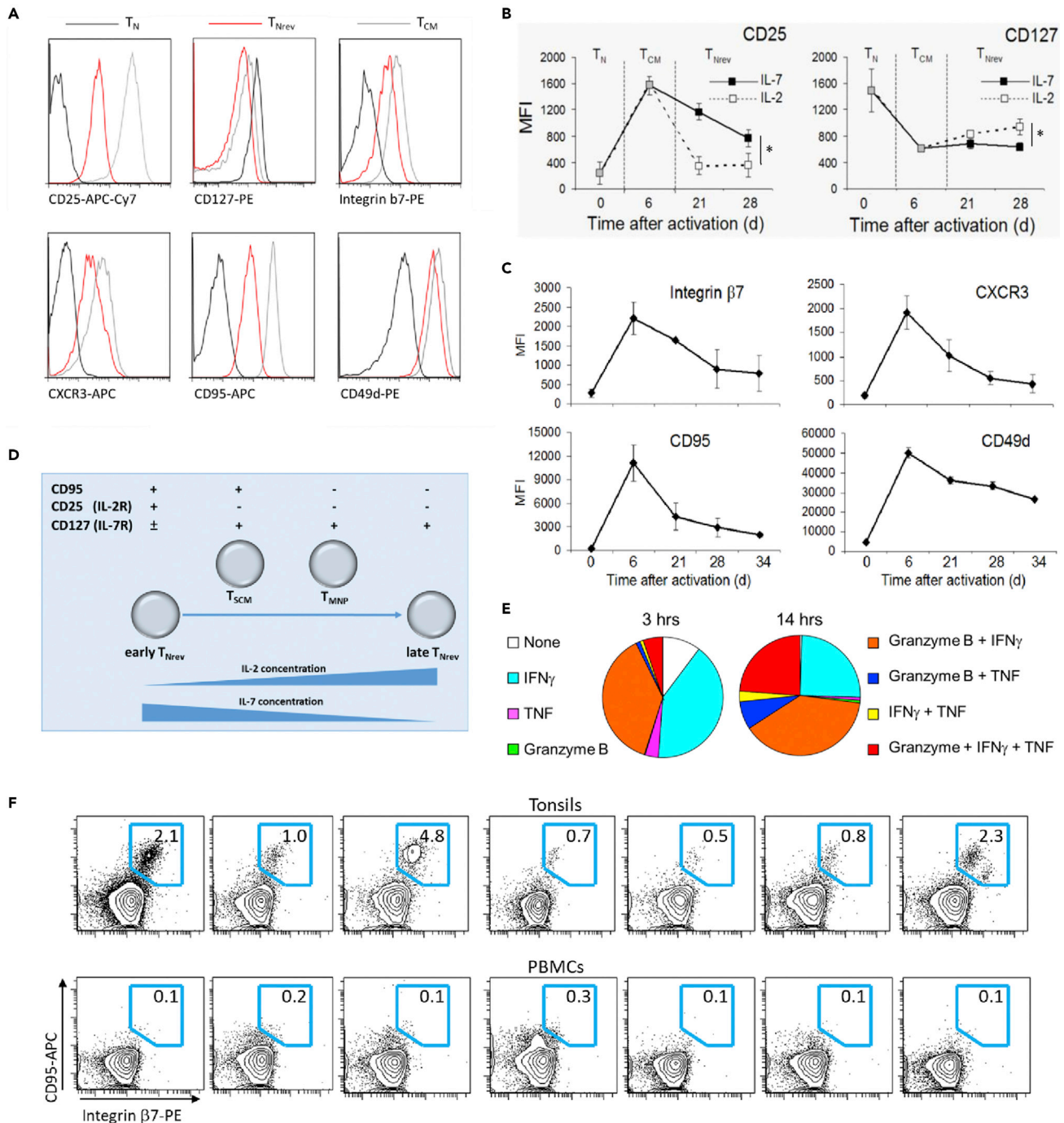


Figure 3. $CD8^+$ T_{Nrev} Can Acquire Phenotypic and Functional Characteristics of Other Early Memory T Cell Subsets and Are Present *In Vivo*

(A) The expression of the markers that discriminate early T_{Nrev} from T_N and recently differentiated T_{CM} was measured by flow cytometry. Single representative experiment out of three.

(B) Kinetics of CD25 and CD127 expression by $CD8^+$ T_{Nrev} in the presence of either IL-2 or IL-7. After phenotype reversion had occurred, cells were either maintained in 25 ng/mL IL-7 or switched to culture in 30 U/mL IL-2. The absence of one cytokine led to increased expression of its cognate receptor. The mean fluorescence intensity (MFI) is shown. Data are represented as means \pm 1SD of three samples. Unpaired t test analysis between the MFI levels at day 28, * = $p < 0.05$.

(C) Kinetics of the expression of discriminatory markers for early T_{Nrev} cells. The MFI was measured at different time points during activation and reversion. Data are represented as means \pm 1SD of three samples.

(D) Scheme of the differences in phenotype between the memory $CD8^+$ T cell subsets showing naive-like phenotype.

Figure 3. Continued

(E) T_{Nrev} were re-stimulated with PMA plus ionomycin, and the percentages of cells expressing granzyme B, IFN γ , TNF- α , and combinations thereof were measured after 3 and 14 h. Data are represented as mean of three samples.

(F) Cells with the T_{Nrev} signature are present among the T_N from tonsils, but not from PB. The expression of CD95 and integrin $\beta 7$ was measured gating CCR7 $^+$ /CD45RA $^+$ CD8 $^+$ T cells from tonsils of seven patients with recurrent acute tonsillitis or from PB of seven unrelated healthy individuals.

profile of CD45RA $^+$ /CCR7 $^+$ /CD27 $^+$ /CD62L $^+$ /CD45RO $^-$ /CXCR3 $^+$ /CD31 $^+$ /CD122 lo . Indeed, the only difference between early T_{Nrev} and the other two subsets was that both T_{MNP} and T_{SCM} express the IL-7 receptor (CD127) and T_{SCM} lack expression of the IL-2 receptor (CD25), whereas T_{Nrev} exhibit a CD127 low CD25 high phenotype. However, expression of the receptors for IL-7 and IL-2 is down-regulated on T cells in the presence of their respective cytokines (Minami et al., 1993; Park et al., 2004; Vranjkovic et al., 2007). When T_{Nrev} were deprived of IL-7 and maintained in IL-2 for 2 weeks they adopted a phenotype almost indistinguishable from T_{SCM} and T_{MNP} with rapid decrease in CD25 expression and progressive increase in CD127 expression (Figure 3B). After an additional 2 weeks of culture with IL-2 there was further progressive loss of CD49d, CD95, CXCR3, and integrin $\beta 7$ (Figure 3C) such that late T_{Nrev} acquire a phenotype approaching that of primary T_N , although their epigenetic signature clearly identifies them as a different population. We were unable to monitor the cells further due to increased cell death. These results suggest that the cytokine milieu and the time since activation account for the modest phenotypic diversity between T_{Nrev} , T_{SCM} , and T_{MNP} (Figure 3D). T_{Nrev} also share functional characteristics with T_{MNP} as the latter cells express granzyme B and secrete IFN γ and TNF- α after re-stimulation with phorbol myristate acetate (PMA) plus ionomycin (Pulko et al., 2016). Resting T_{Nrev} also became polyfunctional after the same treatment, r (Figure 3E).

To assess the *in vivo* relevance of phenotypic reversion we also looked for the presence of cells with the T_{Nrev} signature in the blood and secondary lymphoid tissue (tonsils) of adult donors. CD8 $^+$ T cells with a CCR7 $^{+}$ CD45RA $^+$ naive phenotype and expression of CD95 and integrin $\beta 7$ were present within tonsil but were not seen in blood ($p = 0.017$, unpaired t test, Figure 3F). The population of memory T cells within tonsil had a CD95 low and integrin $\beta 7^{-}$ phenotype (Figure S4) and was clearly distinguishable from the putative T_{Nrev} .

Substantial Chromatin Reorganization Is Observed during Differentiation from T_N to T_{EM} and This Is Partially Retained following Reversion

Epigenetic modifications have a profound regulatory influence on CD8 $^+$ T cell differentiation and function (Henning et al., 2018; Moskowitz et al., 2017). We next used ATAC-seq to investigate the profile of chromatin landscape remodeling during T cell differentiation and reversion. ATAC-seq analysis was performed on purified T_N , T_{CM} , T_{EM} , and T_{Nrev} CD8 $^+$ populations following *in vitro* culture. ATAC-seq read density profiles at phenotype-defining genes such as *CCR7* and *GZMB* were compatible with lineage-specific expression (Figure S5).

Differentially accessible chromatin sites (DACs) were identified within memory subsets and contrasted with the profile in naive cells (Figures 4A and S6A). The majority of epigenetic modifications were acquired relatively late in differentiation during transition from T_{CM} to T_{EM} . In particular, only 26 DACs developed during transition from naive to central memory cells but this increased markedly to 5,829 with further differentiation to T_{EM} . Interestingly, 51% of these DACs were lost during reversion to T_{Nrev} but 2,830 DACs still remained within T_{Nrev} cells (Figures 4A and 4B). Read density distributions at T_{EM} and T_{Nrev} DACs further indicate that the chromatin landscape of T_{Nrev} cells retains similarity to T_{EM} cells (Figures 4C and 4D) and is supported by principal component analysis of sample-wise chromatin accessibility, which identified unique groups for the T_N , T_{CM} , and T_{EM} populations and alignment of T_{Nrev} with the memory subtypes (Figure S6B).

We next investigated the balance of open and closed chromatin during differentiation and reversion. A relative increase in the number of inaccessible chromatin regions was observed during differentiation with 4,316 closed and 1,299 open DACs in T_{EM} compared with T_N (Figure 4E). This profile was retained within the T_{Nrev} population with values of 2,194 and 617 DACs, respectively. The great majority of DACs within T_{Nrev} were shared with the T_{EM} population, although 216 and 546 regions were uniquely open and closed, respectively, within this subtype.

Biochemical Pathways Associated with Reversion Can Be Identified by Epigenomic and Transcriptional Analysis of T Cell Subsets

In order to examine the relationship between chromatin landscape and gene expression, DAC regions were next annotated with the gene whose transcriptional start site was nearest to the peak summit.

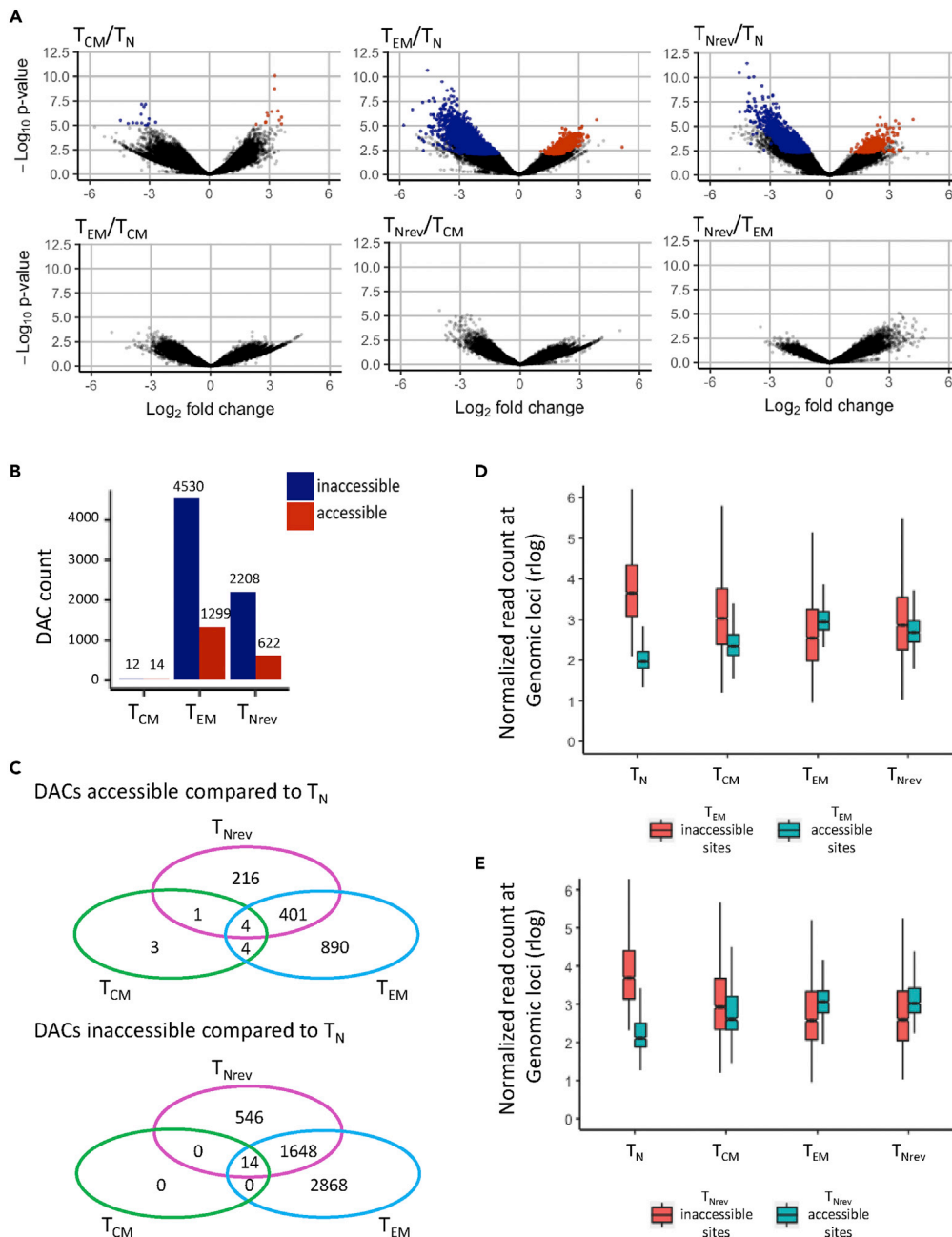


Figure 4. Chromatin Landscape Changes during Differentiation from T_N to T_{CM} and T_{EM} and Reversion to T_{Nrev}

(A) Pairwise comparisons of chromatin accessibility at peak regions. The x axes indicate Log_2 fold change, and the y axes indicate unadjusted $-\text{Log}_{10}$ p value of all peaks. Colored points indicate differentially accessible chromatin sites with inaccessible sites as blue and accessible sites as red.

(B) DACs count for accessible and inaccessible regions in comparison with T_N are shown for T_{CM} , T_{EM} , and T_{Nrev} .

(C) Tracking from T_N to T_{Nrev} the accessibility of DACs becoming inaccessible (T_N to T_{EM} closing)/accessible (T_N to T_{EM} opening) upon differentiation to T_{EM} .

(D) Tracking from T_N to T_{Nrev} the accessibility of DACs becoming inaccessible (T_N to T_{Nrev} closing)/accessible (T_N to T_{Nrev} opening) upon reversion to T_{Nrev} . The y axis is chromatin accessibility in units of rlog normalized mapped reads at the peak site.

(E) Overlaps of differentially accessible sites. Overlaps of DACs more accessible in $T_{CM}/T_{EM}/T_{Nrev}$ compared with T_N (left) and DACs less accessible in $T_{CM}/T_{EM}/T_{Nrev}$ compared with T_N (right).

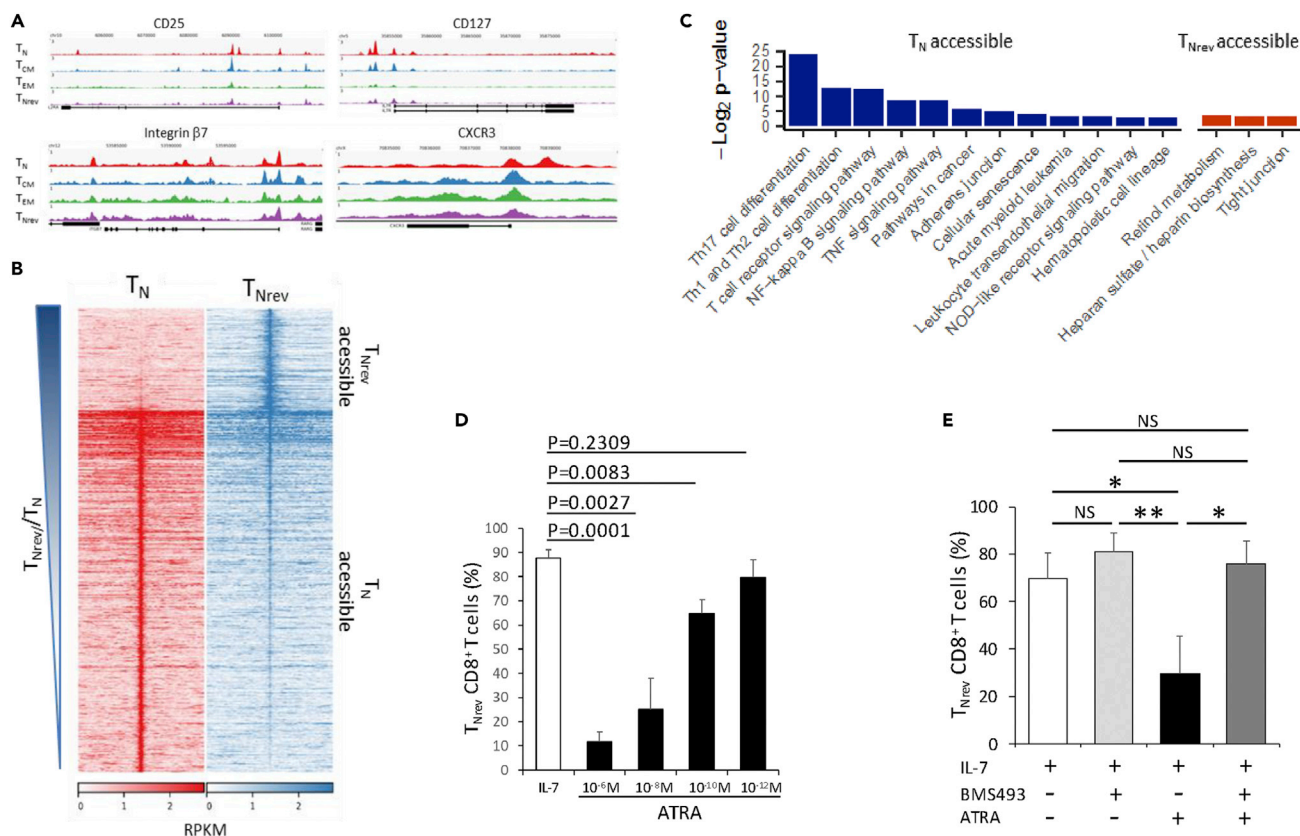


Figure 5. Chromatin Accessibility Identifies Biochemical Pathways Specific for T_N and T_{Nrev}

(A) ATAC-seq signal tracks at selected markers that discriminate early T_{Nrev} from T_N and recently differentiated T_{CM} . Gene diagrams (bottom) show alternative transcripts with black boxes indicating exons. Each subset signal is aggregated across the constituent samples, $n = 4(T_N)$, $3(T_{CM})$, $3(T_{EM})$, $4(T_{Nrev})$. The y axes are in units of reads per million mapped reads.

(B) DAC sites in T_{Nrev} versus T_N cells. Normalized mapped read density (RPKM) of aggregated T_N ($n = 4$) and T_{Nrev} ($n = 4$) mapped ATAC-seq reads at differentially accessible chromatin sites (centered on peak summit, extended ± 5 kbp).

(C) Pathways significantly enriched (adjusted p value < 0.1) in genes closest to T_N accessible or T_{Nrev} accessible DACs.

(D) Efficiency of reversion in the presence of ATRA. The percentage of CD8 $^+$ T_{Nrev} was recorded at day 24 from activation in three CBMC samples. Unpaired t test.

(E) After activation CBMCs were incubated with the indicated combination of IL-7 25 (ng/mL), ATRA (10^{-8} M), and BMS (493.3×10^{-6} M). Data are from three CBMC samples. One-way ANOVA.

As anticipated, differential chromatin accessibility was observed at genes encoding phenotypic markers that discriminate T cell subsets including CD25, CD127, integrin β 7, and CXCR3 (Figure 5A).

Genomic regions enrichment of annotations (GREAT) analysis (Table S2) revealed that the 1,648 DAC sites that became closed in T_{EM} , and were not reopened in T_{Nrev} , were enriched for pathways related to TCR signaling in naive T cells and CXCR4-mediated signaling. Sites that were opened during reversion of T_{EM} to T_{Nrev} showed enrichment for IL-7 signal transduction and Lck/Fyn-mediated initiation of TCR activation, whereas the 546 DAC sites uniquely closed in T_{Nrev} were enriched for pathways involved in generation of T cell cytotoxicity.

To further interrogate the differences between true T_N and T_{Nrev} cells we combined DAC analysis with transcriptional analysis of the two populations. In total 2,830 DAC regions had been identified between the two subtypes, 622 of which were more accessible in T_{Nrev} and 2,208 less accessible (Figure 5B). These regions were annotated with the gene whose transcriptional start site was nearest to the peak summit. Pathway enrichment analysis with g:Profiler highlighted that genes becoming less accessible in T_{Nrev} included those that regulate the major differentiation pathways for Th1, Th2, and Th17 cells (Figure 5C). Genes associated with retinol metabolism became markedly more accessible in T_{Nrev} , and is of note given the pleiotropic

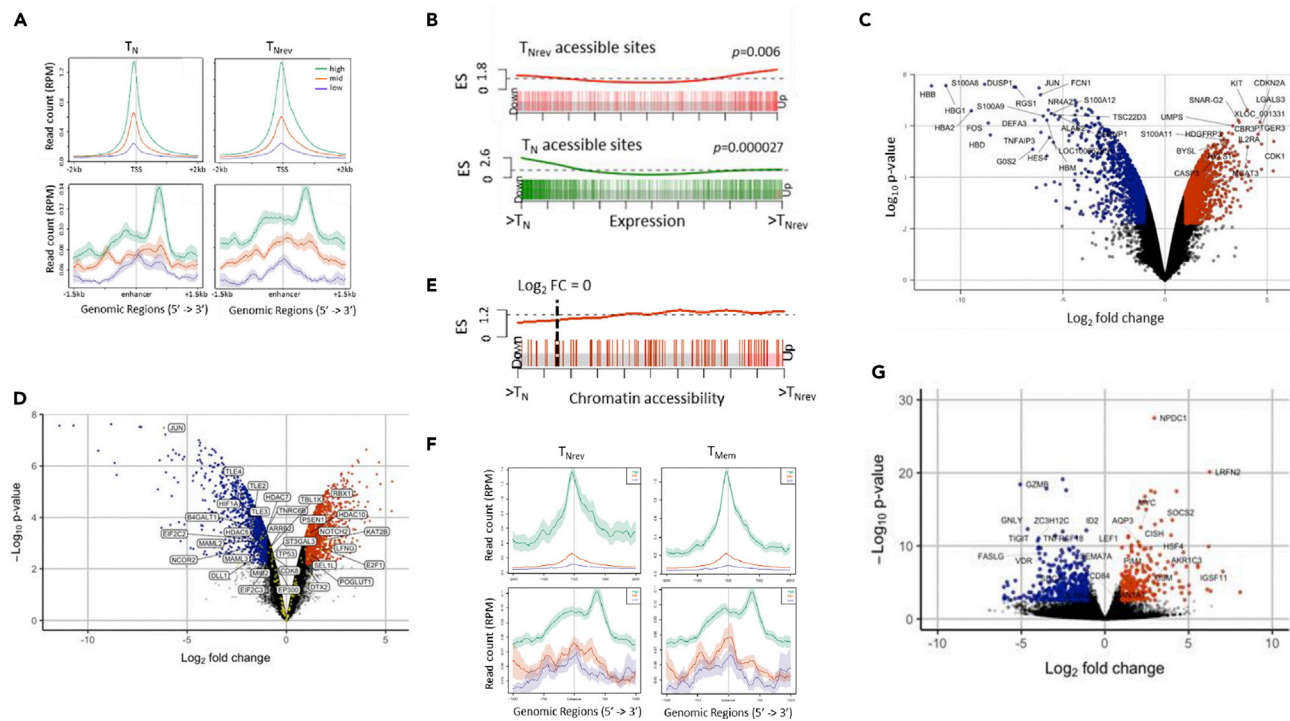


Figure 6. Chromatin Accessibility and Transcriptome Profiles of T_N and T_{Nrev}

(A) Average mapped read density profiles (centered on TSS (top) and enhancer regions (bottom)) generated from aggregated T_N (left) and T_{Nrev} (right) ATAC-seq reads. Profiles are for genes identified from transcriptome analysis to be expressed at low, medium, and high levels in T_N and T_{Nrev} cells, respectively. (B) Enrichment score (ES) for gene expression changing coordinately with chromatin accessibility. ES of genes closest to T_{Nrev} accessible (red) and T_N accessible (green) DACs, vertical bars indicate position of such genes on the axis of fold change in expression (ranking from most down-regulated in T_{Nrev} to most up regulated in T_{Nrev}).

(C) Microarray analysis was performed on three $CD8^+$ T_N samples and on the respective $CD8^+$ T_{Nrev} cells. Pairwise comparison of gene expression in T_N versus T_{Nrev} cells showing $-\text{Log}_2 p$ value versus Log_2 fold change of all genes. Colored points indicate differentially expressed genes that are down-regulated in T_{Nrev} (blue) and up-regulated in T_{Nrev} (orange).

(D) The genes in the Notch pathway (yellow dots) that are significantly down-regulated and up-regulated in T_{Nrev} are labeled.

(E) Barcode plot from GSEA analysis showing ES of Notch signaling genes within sites ranked by chromatin accessibility. Vertical bars indicate position of such genes on the axis of fold change in chromatin accessibility, ranking from most inaccessible in T_{Nrev} to most up accessible in T_{Nrev} .

(F) As in (A) but for aggregated T_{Nrev} (left) and T_{Mem} (right) ATAC-seq reads.

(G) RNA-seq analysis was performed on four T_{Mem} samples (two T_{CM} and two T_{EM}) and on the respective $CD8^+$ T_{Nrev} cells. Pairwise comparison of gene expression in T_N versus T_{Nrev} cells showing $-\text{Log}_2 p$ value versus Log_2 fold change of all genes. Colored points indicate differentially expressed genes that are down-regulated in T_{Nrev} (blue) and up-regulated in T_{Nrev} (orange).

effects on retinoic acid on T cell differentiation (Beijer et al., 2013). Indeed, escalating doses of all-trans retinoic acid (ATRA) progressively inhibited reversion of IL-7-treated $CD8^+$ T cells (Figure 5D) and this was blocked by a pan-retinoic acid receptor antagonist (Figure 5E).

Transcriptional analysis confirmed that RNA expression levels were strongly associated with ATAC-seq read density at transcription start sites and enhancer regions (Figure 6A), and enrichment analysis of gene sets annotated at T_{Nrev} DACs confirmed strong relationship between chromatin accessibility and expression level (Figure 6B). Transcriptome analysis revealed 2,841 differentially expressed genes including major immune regulators such as *FOS*, *JUN*, *KIT*, and *IL2RA* (Figures 6C and 6F and Table S3). Moreover, 32 of the 104 genes within the Notch signaling pathway were differentially regulated in T_{Nrev} (Figures 6D and 6G). Gene set enrichment analysis (GSEA) of regions closest to Notch signaling genes confirmed an enrichment in accessible chromatin regions in T_{Nrev} cells (Figure 6E) particularly in the *HDAC2* and *HDAC9*-associated regions.

Comparative transcriptional analysis of T_{Nrev} with memory T cells (T_{Mem}) (Figures S7A–S7C) also confirmed RNA expression to be associated with ATAC-seq read density (Figure 6F), and pairwise comparison

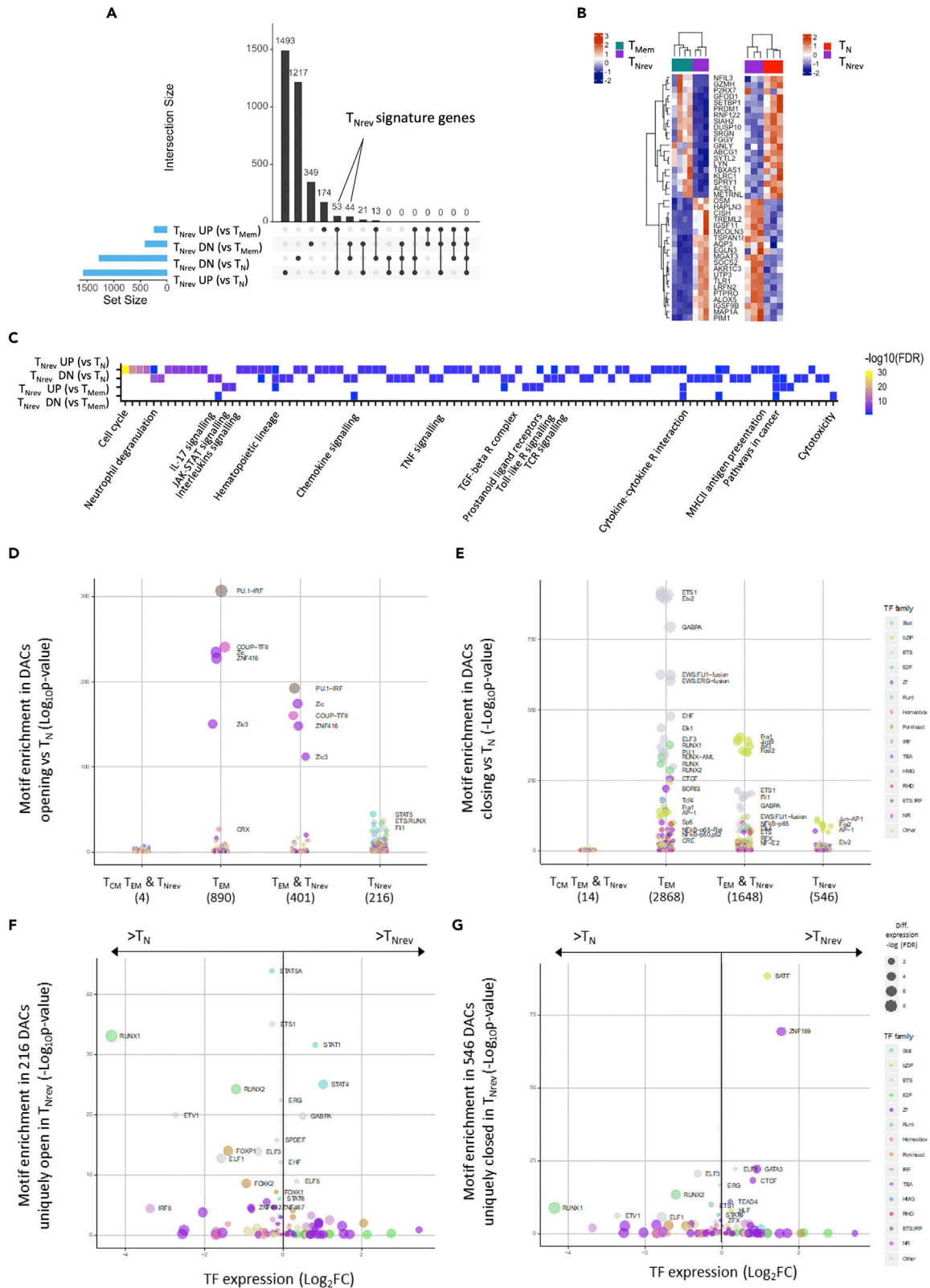


Figure 7. Transcriptional Signatures of T_{Nrev} Cells

- (A) Intersections of DEGs identified from differential expression analysis of T_{Nrev} versus T_{Mem} and T_{Nrev} versus T_N .
 (B) Heatmap of the top 40 T_{Nrev} signature genes. Z-scores were calculated for each gene from RNA-seq (left) and Microarray (right) datasets independently.
 (C) Significant (FDR<0.1) pathway enrichments identified within DEG lists from T_{Nrev} versus T_{Mem} and T_{Nrev} versus T_N .
 (D) TF-binding motif enrichments at DACs more accessible compared with T_N . Motif enrichments were calculated on the following DACs: 4 shared in T_{CM} , T_{EM} and T_{Nrev} ; 890 in T_{EM} ; 401 shared in T_{EM} and T_{Nrev} ; 216 in T_{Nrev} .
 (E) TF-binding motif enrichments at DACs less accessible compared with T_N . Motif enrichments were calculated on the following DACs: 14 shared in T_{CM} , T_{EM} , and T_{Nrev} ; 2,868 in T_{EM} ; 1,648 shared in T_{EM} and T_{Nrev} ; 546 in T_{Nrev} .
 (F) Expression of TFs with binding motifs enriched in loci that are uniquely open in T_{Nrev} cells. The x axis indicates fold change in TF expression, and the y axis indicates $-\log_{10}$ p value of TF-binding motif enrichment in loci uniquely more accessible in T_{Nrev} cells. Increasing dot size indicates increasingly significant difference in TF expression and color indicates TF family.
 (G) As in (D) but for TFs with binding motifs enriched in loci uniquely closed after reversion to T_{Nrev} .

revealed 447 genes down-regulated in T_{Nrev} including several involved in T cell cytolytic activity such as *GZMB*, *GZMH*, and *GNLY*. In contrast, 267 genes were up-regulated and included proteins that support cell survival and act to block cell differentiation, such as *CISH*, *NPDC1*, *HSF4*, and *OSM* (Figure 6G). Interrogation of the transcriptomes of T_{Nrev} , T_{Mem} , and T_N subsets allowed identification of 97 signature genes specific for T_{Nrev} (Figures 7A and 7B) and pathways enriched in genes that were differentially regulated in this subset (Figure 7C). These include a number of intracellular signaling pathways, such as JAK-STAT and the RUNX-dependent regulation of WNT signaling. Comparison of TF transcripts in T_{Nrev} and T_{Mem} (Figure S8) showed differences in the expression of TFs related to stemness and generation of T_{SCM} (Gattinoni et al., 2012; Kondo et al., 2018).

Reversion Is Associated with Opening of Binding Sites for RUNX and STAT Transcription Factors and Closure of Sites that Bind BATF

TFs can instigate chromatin remodeling and act as important regulators of differentiation. As such, we next assessed the relative enrichment of TF-binding motifs within genomic regions that became differentially open or closed in the different cell subsets. DACs that became more accessible in T_{EM} were enriched in binding motifs for five TF complexes, including PU.1/IRF, COUP-TFII, and zinc finger members, and these open sites were largely retained during reversion to T_{Nrev} cells (Figures 7D and 7E). In contrast, many TF-binding motifs became less accessible upon differentiation to T_{EM} although this profile was not strongly retained in the T_{Nrev} subset.

Finally, in order to gain insight into the potential regulators of reversion we focused on the relative access of TFs for regions of chromatin that were uniquely open or closed in T_{Nrev} cells. Strikingly, chromatin regions containing binding motifs for ET1, RUNX1, and RUNX2, as well as STAT1, STAT4, and STAT5, all became more accessible during reversion, although transcriptional activity from RUNX1 and RUNX2 genes was suppressed in the revertant population (Figure 7F and Table S4). In contrast, there was substantial closure of chromatin regions containing binding motifs for BATF and ZNF189 (Figure 7G and Table S4), which is of particular note given the importance of BATF in driving PD-1-mediated T cell exhaustion (Wherry, 2011).

DISCUSSION

There is increasing appreciation of the importance of cellular plasticity (Blanpain and Fuch, 2014), and reversion of mature cells into stem cells has been confirmed in some organ systems (Stange et al., 2013; Tata et al., 2013). Here we show that extensive phenotypic reversion of effector $CD8^+$ T cells to naive phenotype can occur within the human immune system. Reversion was mediated primarily by IL-7, which is expressed by a range of stromal cells within secondary lymphatic organs and is therefore available to support reversion following local antigen-driven activation (Huang and Luther, 2012). Indeed, cells with a T_{Nrev} phenotype were located within human tonsil. An interesting observation was that the addition of IL-7 markedly decreased apoptosis, suggesting that reversion may be a “default” pathway of recently activated T_N cells in the presence of appropriate survival signals (Hong et al., 2012; Mackall et al., 2011; Surh and Sprent, 2008).

The finding sheds light on the potential relationship between the T_{SCM} , T_{MNP} , and T_{Nrev} populations. These three groups share a common core phenotype exemplified by expression of CD45RA, CCR7, and CXCR3. CD45RA regulates the signaling threshold in T lymphocytes (Hermiston et al., 2003; Irles et al., 2003), and CCR7 permits entry into secondary lymphoid tissue, whereas CXCR3 plays a fundamental role in extravasation of $CD8^+$ T cells into inflammatory sites (Cole et al., 1998; Mikucki et al., 2015; Peperzak et al., 2013).

The naive-memory phenotype therefore generates an antigen-specific memory pool, which retains the ability to enter lymphoid tissue but has developed heightened responsiveness to re-challenge and may gain rapid access to tissue sites.

Interestingly, the major differences in the phenotype of T_{Nrev} , T_{SCM} , and T_{MNP} relate to expression of the IL-7 and IL-2 receptors and these were modulated on T_{Nrev} according to the local concentration of IL-2 and IL-7 (Minami et al., 1993; Park et al., 2004; Vranjkovic et al., 2007). T_{SCM} also express CD95⁺, whereas T_{MNP} express CD49d, and we observed that both receptors are down-regulated during prolonged incubation, with CD95 expression falling more rapidly than CD49d expression. As such, we would suggest that the three populations represent a spectrum of naive-memory cells that are generated by reversion and display modest phenotypic diversity that varies according to cytokine concentration and time since activation. Indeed, phenotypic transition of T_{EM} to T_{CM} populations has been observed in murine systems (Wherry et al., 2003), and reversion from T_{EM} to T_{CM} and from these subsets to T_{SCM} was described in patients following hematopoietic stem cell transplant (Cieri et al., 2015).

This work builds on the work of Cieri et al. who previously demonstrated the generation of T_{SCM} from naive cells after T cell engagement in the presence of IL-7. However, in that study the cytokine was included in culture from the start of activation. We certainly do not rule out the possibility that T_{MNP} and T_{SCM} may also be generated by additional mechanisms such as direct differentiation from T_N (Cieri et al., 2013; Lugli et al., 2013; Sabatino et al., 2016; Zanon et al., 2017) and CD8⁺ T_{SCM} have also been induced *in vitro* by activation of T cells in the presence of a glycogen synthase-3 β inhibitor (Sabatino et al., 2016). Engagement of the Notch pathway in memory T cells also generates T_{SCM} -like CD8⁺ and CD4⁺ T cells (Kondo et al., 2017), and we found a number of genes in the Notch pathway to be differently expressed between T_N and T_{Nrev} (Figure 6D). Furthermore, IL-7 can further enhance with Notch signaling to induce a T_N -like phenotype in recently activated CD8⁺ T cells (Kondo et al., 2018). These findings suggest that notch engagement and IL-7 may represent two alternative mechanisms to generate T_{SCM} -like cells.

Importantly, we observed that T_{Nrev} cells were able to undergo several rounds of reversion *in vitro*, and as such this process may be important in protection from both acute and chronic infectious agents. Indeed, it is now clear that a substantial proportion of antigen-experienced T cells is contained within the apparent “naive” CD8⁺ T cell pool (Ellefsen et al., 2002; Remmerswaal et al., 2012). Longer-term culture of T_{Nrev} led to progressive down-regulation of integrin β 7 and CXCR3, but it is uncertain if they can ultimately acquire a phenotype indistinguishable from that of primary T_N .

Most of our work was performed on T cells from CB, which contains very few memory or effector cells. We did observe phenotypic reversion using T_N cells from adult donors, although the relative proportion of cells that underwent reversion was sharply reduced and may reflect the decreased number of open chromatin sites and binding sites for TF in adult PB. Interestingly, the epigenetic landscape of CD8⁺ T cells in older people is globally biased toward a differentiated phenotype (Moskowitz et al., 2017) with a reduction in chromatin accessibility that is most apparent at the IL-7R locus (Ucar et al., 2017).

Phenotypic reversion may help to explain the paradox of preservation of the human T_N pool during aging despite *in vivo* analyses and mathematical modeling suggesting that thymic output is insufficient for its maintenance (den Braber et al., 2012; Hakim et al., 2005; Murray et al., 2003). Interestingly, it was found that the T_{SCM}/T_N ratio in PB increases with age (Li et al., 2019), suggesting that during aging naive-memory cells replace T_N and sustain immunological memory.

Epigenetic regulation maintains the equilibrium between self-renewal and differentiation of stem cells and regulates tissue homeostasis throughout life. As such we were keen to understand how the chromatin landscape was modified following T cell activation and if these changes were reversible during phenotypic reversion to T_{Nrev} . Interestingly, this was largely not the case and T_{Nrev} cells retained an epigenetic profile that was similar to effector cells. As such, T_{Nrev} become “epigenetically primed” for secondary activation at the same time as they undergo phenotypic reversion to a naive-memory phenotype. The chromatin modifications within T_{Nrev} are likely to explain their ability to rapidly differentiate and acquire effector function in response to secondary stimulation and reveal a discrepancy between the degree of phenotypic and epigenetic reversion. This may partly explain the decrease in chromatin accessibility in phenotypically naive CD8⁺ T cells in older people (Ucar et al., 2017). Furthermore, the observation that the chromatin landscape

of T_{Nrev} is much more extensively modified than that of T_{CM} provides further confirmation that they have undergone sequential differentiation and reversion rather than minimal differentiation from T_N .

Analysis of the distribution of TF-binding sites within differentially accessible chromatin regions can help to identify potential transcriptional regulators of differentiation. A striking observation was that many chromatin regions containing binding sites for BATF became closed during reversion. BATF is an essential regulator of $CD8^+$ differentiation (Kurachi et al., 2014), and PD-1 engagement on T cells can drive BATF-dependent terminal differentiation (Quigley et al., 2010).

Reversion may play a potential role in limiting T cell exhaustion in both physiological and pathological settings, and it is noteworthy that the chromatin region containing the *IL-7R* gene becomes poorly accessible in exhausted $CD8^+$ cells (Scott-Browne et al., 2016). In contrast, chromatin regions enriched for binding sites of several TFs, including RUNX, STAT, and ETS family members, became more accessible within revertant subsets. Stat1 and Stat4 signaling regulate T cell responses to interferon and cytokine signaling (Gil et al., 2006; Nguyen et al., 2002; Thierfelder et al., 1996), STAT5 is critical in maintaining effector $CD8$ T cell responses (Tripathi et al., 2010), and over-representation of ETS motifs in chromatin accessible regions has been observed previously in naive T cells (Moskowitz et al., 2017). As such the “epigenetic priming” of naive-memory subsets appears to reflect an increased sensitivity to interferon and cytokines within the local microenvironment but protection from terminal differentiation.

Cytokine-driven reversion of recently activated $CD8^+$ T cells thus uncovers a novel pathway for T cell differentiation and provides a unifying hypothesis for the existence of a naive-memory pool that contains T_{SCM} , T_{MNP} , and T_{Nrev} populations. We also show that the chromatin structure of naive-revertant cells is substantially reorganized in comparison with the naive pool and as such they are epigenetically “primed for secondary activation. These observations will help to guide studies of fundamental mechanisms that regulate T cell differentiation and should also be of considerable value for optimal generation of naive-memory cells for adoptive T cell immunotherapy as less differentiated cells have been associated with superior engraftment, persistence, and antitumor activity (Hinrichs et al., 2011; Klebanoff et al., 2011).

Limitations of the Study

A few limitations should be considered when interpreting our data. Although we identified cells with the phenotype of T_{Nrev} cells in human tonsil, it will be of interest to assess further if these are generated directly *in vivo*. In addition, it will be important to pursue parallel studies within animal models to interrogate potential mechanisms of phenotypic reversion.

METHODS

All methods can be found in the accompanying [Transparent Methods supplemental file](#).

DATA AND CODE AVAILABILITY

All relevant data are available from the authors upon request. RNA sequencing data have been deposited in Gene Expression Omnibus, accession number GSE114812.

SUPPLEMENTAL INFORMATION

Supplemental Information can be found online at <https://doi.org/10.1016/j.isci.2020.100989>.

ACKNOWLEDGMENTS

We thank Yvonne Caffrey and the staff of the NHS Cord Blood Bank, Colindale, UK, for providing CB units; Richard Brain and the staff of the Blood Donor Center, NHSBT, Birmingham, UK, for providing blood samples; and David Briggs and the staff of Cellular and Molecular Therapies, NHSBT, Birmingham, UK, for laboratory support. We thank Steve Lee for providing the construct for TCR gene transduction and Paul Murray and Eszter Nagy for providing mononuclear cells from tonsils. We also thank Peter Cockerill, Sarah Bevington, and Celina Whalley for suggestions on ATAC sequencing. We are grateful to Dr Geoff Brown for advice on the use of ATRA. RNA-seq was carried out by Edinburgh Genomics, The University of Edinburgh, Edinburgh, UK. Genomics is partly supported through core grants from NERC (R8/H10/56), MRC (MR/K001744/1), and BBSRC (BB/J004243/1). This work was supported by grants from Bloodwise (12052), MRC (MR/K021192/1, MR/N000919/1 and MC PC 15079), and NIHR UK (RP-PG-0310-10003).

AUTHOR CONTRIBUTIONS

G.F. designed and performed experiments, interpreted the data, and wrote the paper; K.V. performed the ATAC-seq experiments and wrote the paper; W.C. analyzed microarray data and ATAC-seq data and wrote the paper; A.W. performed part of flow cytometry experiments; Z.N. analyzed microarray data; S.K. performed gene expression analysis; G.A. advised on experiments and edited the paper; P.M. and F.E.C. interpreted the data, supervised the study, and wrote the paper.

DECLARATION OF INTERESTS

The authors declare no competing interests.

Received: September 3, 2019

Revised: December 9, 2019

Accepted: March 11, 2020

Published: April 24, 2020

REFERENCES

- Beijer, M., Molenaar, R., Goversek, G., Mebius, R.E., Kraal, G., and den Haan, J.M. (2013). A crucial role for retinoic acid in the development of Notch-dependent murine splenic CD8- CD4- and CD4+ dendritic cells. *Eur. J. Immunol.* 43, 1608–1616.
- Blanpain, C., and Fuch, E. (2014). Stem cell plasticity. Plasticity of epithelial stem cells in tissue regeneration. *Science* 344, 1242281.
- Christensen, J.E., Andreassen, S.O., Christensen, J.P., and Thomsen, A.R. (2001). CD11b expression as a marker to distinguish between recently activated effector CD8⁺ T cells and memory cells. *Int. Immunol.* 13, 593–600.
- Cieri, N., Camisa, B., Cocchiarella, F., Forcato, M., Oliveira, G., Provasi, E., Bondanza, A., Bordignon, C., Peccatori, J., Ciceri, F., et al. (2013). IL-7 and IL-15 instruct the generation of human memory stem T cells from naive precursors. *Blood* 121, 573–584.
- Cieri, N., Oliveira, G., Greco, R., Forcato, M., Taccioli, C., Cianciotti, B., Valtolina, V., Noviello, M., Vago, L., Bondanza, A., et al. (2015). Generation of human memory stem T cells after haploidentical T-replete hematopoietic stem cell transplantation. *Blood* 125, 2865–2874.
- Cole, K.E., Strick, C.A., Paradis, T.J., Osborne, K.T., Loetscher, M., Gladue, R.P., Lin, W., Boyd, J.G., Moser, B., Wood, D.E., et al. (1998). Interferon-inducible T cell alpha chemoattractant (I-TAC): a novel non-ELR CXC chemokine with potent activity on activated T cells through selective high affinity binding to CXCR3. *J. Exp. Med.* 187, 2009–2021.
- den Braber, I., Mugwagwa, T., Vriskoop, N., Westera, L., Mögling, R., de Boer, A.B., Willems, N., Schrijver, E.H., Spierenburg, G., Gaiser, K., et al. (2012). Maintenance of peripheral naive T cells is sustained by thymus output in mice but not humans. *Immunity* 36, 288–297.
- Ellefsen, K., Harari, A., Champagne, P., Bart, P.A., Sékaly, R.P., and Pantaleo, G. (2002). Distribution and functional analysis of memory antiviral CD8 T cell responses in HIV-1 and cytomegalovirus infections. *Eur. J. Immunol.* 32, 3756–3764.
- Frumento, G., Zheng, Y., Aubert, G., Raeiszadeh, M., Lansdorp, P.M., Moss, P., Lee, S.P., and Chen, F.E. (2013). Cord blood T cells retain early differentiation phenotype suitable for immunotherapy after TCR gene transfer to confer EBV specificity. *Am. J. Transpl.* 13, 45–55.
- Gattinoni, L., Lugli, E., Ji, Y., Pos, Z., Paulos, C.M., Quigley, M.F., Almeida, J.R., Gostick, E., Yu, Z., Carpenito, C., et al. (2011). A human memory T cell subset with stem cell-like properties. *Nat. Med.* 17, 1290–1297.
- Gattinoni, L., Klebanoff, C.A., and Restifo, N.P. (2012). Paths to stemness: building the ultimate antitumor T cell. *Nat. Rev. Cancer* 12, 671–684.
- Gattinoni, L., Speiser, D.E., Lichterfeld, M., and Bonini, C. (2017). T memory stem cells in health and disease. *Nat. Med.* 23, 18–27.
- Gil, M.P., Salomon, R., Louten, J., and Biron, C.A. (2006). Modulation of STAT1 protein levels: a mechanism shaping CD8 T-cell responses in vivo. *Blood* 107, 987–993.
- Hakim, F.T., Memon, S.A., Cepeda, R., Jones, E.C., Chow, C.K., Kasten-Sportes, C., Odom, J., Vance, B.A., Christensen, B.L., Mackall, C.L., et al. (2005). Age-dependent incidence, time course, and consequences of thymic renewal in adults. *J. Clin. Invest.* 115, 930–939.
- Hendriks, J., Xiao, Y., and Borst, J. (2003). CD27 promotes survival of activated T cells and complements CD28 in generation and establishment of the effector T cell pool. *J. Exp. Med.* 198, 1369–1380.
- Henning, A.N., Roychoudhuri, R., and Restifo, N.P. (2018). Epigenetic control of CD8⁺ T cell differentiation. *Nat. Rev. Immunol.* 18, 340–356.
- Hermiston, M.L., Xu, Z., and Weiss, A. (2003). CD45: a critical regulator of signaling thresholds in immune cells. *Annu. Rev. Immunol.* 21, 107–137.
- Hinrichs, C.S., Borman, Z.A., Gattinoni, L., Yu, Z., Burns, W.R., Huang, J., Klebanoff, C.A., Johnson, L.A., Kerkar, S.P., Yang, S., et al. (2011). Human effector CD8⁺ T cells derived from naive rather than memory subsets possess superior traits for adoptive immunotherapy. *Blood* 117, 808–814.
- Hong, C., Luckey, M.A., and Park, J.H. (2012). Intrathymic IL-7: the where, when, and why of IL-7 signaling during T cell development. *Semin. Immunol.* 24, 151–158.
- Huang, H.Y., and Luther, S.A. (2012). Expression and function of interleukin-7 in secondary and tertiary lymphoid organs. *Semin. Immunol.* 24, 175–189.
- Irles, C., Symons, A., Michel, F., Bakker, T.R., van der Merwe, P.A., and Acuto, O. (2003). CD45 ectodomain controls interaction with GEMs and Lck activity for optimal TCR signaling. *Nat. Immunol.* 4, 189–197.
- Ishida, Y., Agata, Y., Shibahara, K., and Honjo, T. (1992). Induced expression of PD-1, a novel member of the immunoglobulin gene superfamily, upon programmed cell death. *EMBO J.* 11, 3887–3895.
- Kim, E.Y., Priel, J.J., The, S.J., and The, H.S. (2006). TNF receptor type 2 (p75) functions as a costimulator for antigen-driven T cell responses in vivo. *J. Immunol.* 176, 1026–1035.
- Klebanoff, C.A., Gattinoni, L., and Restifo, N.P. (2006). CD8⁺ T-cell memory in tumor immunology and immunotherapy. *Immunol. Rev.* 211, 214–224.
- Klebanoff, C.A., Gattinoni, L., and Restifo, N.P. (2011). Sorting through subsets: which T-cell populations mediate highly effective adoptive immunotherapy? *J. Immunother.* 35, 651–660.
- Kondo, T., Morita, R., Okuzono, Y., Nakatsukasa, H., Sekiya, T., Chikuma, S., Shichita, T., Kanamori, M., Kubo, M., Koga, K., et al. (2017). Notch-mediated conversion of activated T cells into stem cell memory-like T cells for adoptive immunotherapy. *Nat. Commun.* 8, 15338.
- Kondo, T., Imura, Y., Chikuma, S., Hibino, S., Omata-Mise, S., Ando, M., Akanuma, T., Iizuka, M., Sakai, R., Morita, R., et al. (2018). Generation and application of human induced-stem cell memory T cells for adoptive immunotherapy. *Cancer Sci.* 109, 2130–2140.
- Kurachi, M., Barnitz, R.A., Yosef, N., Odorizzi, P.M., Di Iorio, M.A., Lemieux, M.E., Yates, K., Godec, J., Klatt, M.G., Regev, A., et al. (2014). The

transcription factor BATF operates as an essential differentiation checkpoint in early effector CD8⁺ T cells. *Nat. Immunol.* 15, 373–383.

Li, M., Yao, D., Zeng, X., Kasakovski, D., Zhang, Y., Chen, S., Zha, X., Li, Y., and Xu, L. (2019). Age related human T cell subset evolution and senescence. *Immun. Ageing* 16, 24.

Lugli, E., Dominguez, M.H., Gattinoni, L., Chattopadhyay, P.K., Bolton, D.L., Song, K., Klatt, N.R., Brenchley, J.M., Vaccari, M., Gostick, E., et al. (2013). Superior T memory stem cell persistence supports long-lived T cell memory. *J. Clin. Invest.* 123, 594–599.

Mackall, C.L., Fry, T.J., and Gress, R.E. (2011). Harnessing the biology of IL-7 for therapeutic application. *Nat. Rev. Immunol.* 11, 330–342.

Mikucki, M.E., Fisher, D.T., Matsuzaki, J., Skitzki, J.J., Gaulin, N.B., Muhitch, J.B., Ku, A.W., Frelinger, J.G., Odunsi, K., Gajewski, T.F., et al. (2015). Non-redundant requirement for CXCR3 signalling during tumoricidal T-cell trafficking across tumour vascular checkpoints. *Nat. Commun.* 6, 7458.

Minami, Y., Kono, T., Miyazaki, T., and Taniguchi, T. (1993). The IL-2 receptor complex: its structure, function, and target genes. *Annu. Rev. Immunol.* 11, 245–268.

Moskowitz, D.M., Zhang, D.W., Hu, B., Le Saux, S., Yanes, R.E., Ye, Z., Buenostro, J.D., Weyand, C.M., Greenleaf, W.J., and Goronzy, J.J. (2017). Epigenomics of human CD8 T cell differentiation and aging. *Sci. Immunol.* 2, eaag0192.

Murray, J.M., Kaufmann, G.R., Hodgkin, P.D., Lewin, S.R., Kelleher, A.D., Davenport, M.P., and Zaunders, J.J. (2003). Naive T cells are maintained by thymic output in early ages but by proliferation without phenotypic change after age twenty. *Immunol. Cell. Biol.* 81, 487–495.

Nguyen, K.B., Watford, W.T., Salomon, R., Hofmann, S.R., Pien, G.C., Morinobu, A., Gadina, M., O’Shea, J.J., and Biron, C.A. (2002). Critical role for STAT4 activation by type 1 interferons in the interferon-gamma response to viral infection. *Science* 297, 2063–2066.

O’Shea, J.J., McVicar, D.W., Bailey, T.L., Burns, C., and Smyth, M.J. (1992). Activation of human peripheral blood T lymphocytes by pharmacological induction of protein-tyrosine

phosphorylation. *Proc. Natl. Acad. Sci. U S A* 89, 10306–10310.

Park, J.H., Yu, Q., Erman, B., Appelbaum, J.S., Montoya-Durango, D., Grimes, H.L., and Singer, A. (2004). Suppression of IL7 α transcription by IL-7 and other prosurvival cytokines: a novel mechanism for maximizing IL-7-dependent T cell survival. *Immunity* 21, 289–302.

Peperzak, V., Veraar, E.A., Xiao, Y., Babala, N., Thiadens, K., Brugmans, M., and Borst, J. (2013). CD8⁺ T cells produce the chemokine CXCL10 in response to CD27/CD70 costimulation to promote generation of the CD8⁺ effector T cell pool. *J. Immunol.* 191, 3025–3036.

Pulko, V., Davies, J.S., Martinez, C., Lanteri, M.C., Busch, M.P., Diamond, M.S., Knox, K., Bush, E.C., Sims, P.A., Sinari, S., et al. (2016). Human memory T cells with a naive phenotype accumulate with aging and respond to persistent viruses. *Nat. Immunol.* 17, 966–975.

Quigley, M., Pereyra, F., Nilsson, B., Porichis, F., Fonseca, C., Eichbaum, Q., Julg, B., Jesneck, J.L., Brosnahan, K., Imam, S., et al. (2010). Transcriptional analysis of HIV-specific CD8⁺ T cells shows that PD-1 inhibits T cell function by upregulating BATF. *Nat. Med.* 16, 1147–1151.

Remmerswaal, E.B., Havenith, S.H., Idu, M.M., van Leeuwen, E.M., van Donselaar, K.A., Ten Brinke, A., van der Bom-Baylon, N., Bemelman, F.J., van Lier, R.A., and Ten Berge, I.J. (2012). Human virus-specific effector-type T cells accumulate in blood but not in lymph nodes. *Blood* 119, 1702–1712.

Sabatino, M., Hu, J., Sommariva, M., Gautam, S., Fellowes, V., Hocker, J.D., Dougherty, S., Qin, H., Klebanoff, C.A., Fry, T.J., et al. (2016). Generation of clinical-grade CD19-specific CAR-modified CD8⁺ memory stem cells for the treatment of human B-cell malignancies. *Blood* 128, 519–528.

Scott-Browne, J.P., López-Moyado, I.F., Trifari, S., Wong, V., Chavez, L., Rao, A., and Pereira, R.M. (2016). Dynamic changes in chromatin accessibility occur in CD8⁺ T cells responding to viral infection. *Immunity* 45, 1327–1340.

Stange, D.E., Koo, B.K., Huch, M., Sibbel, G., Basak, O., Lyubimova, A., Kujala, P., Bartfeld, S., Koster, J., Geahlen, J.H., et al. (2013). Differentiated troy(+) chief cells act as reserve stem cells to generate all lineages of the stomach epithelium. *Cell* 155, 357–368.

Surh, C.D., and Sprent, J. (2008). Homeostasis of naive and memory T cells. *Immunity* 29, 848–862.

Tata, P.R., Mou, H., Pardo-Saganta, A., Zhao, R., Prabhu, M., Law, B.M., Vinarsky, V., Cho, J.L., Breton, S., Sahay, A., et al. (2013). Dedifferentiation of committed epithelial cells into stem cells in vivo. *Nature* 503, 218–223.

Thierfelder, W.E., van Deursen, J.M., Yamamoto, K., Tripp, R.A., Sarawar, S.R., Carson, R.T., Sangster, M.Y., Vignali, D.A., Doherty, P.C., Grosveld, G.C., et al. (1996). Requirement for Stat4 in interleukin-12-mediated responses of natural killer and T cells. *Nature* 382, 171–174.

Tripathi, P., Kurtulus, S., Wojciechowski, S., Sholl, A., Hoebe, K., Morris, S.C., Finkelman, F.D., Grimes, H.L., and Hildeman, D.A. (2010). STAT5 is critical to maintain effector CD8⁺ T cell responses. *J. Immunol.* 185, 2116–2124.

Ucar, D., Márquez, E.J., Chung, C.H., Marches, R., Rossi, R.J., Uyar, A., Wu, T.C., George, J., Stitzel, M.L., Palucka, A.K., et al. (2017). The chromatin accessibility signature of human immune aging stems from CD8⁺ T cells. *J. Exp. Med.* 214, 3123–3144.

Vranjkovic, A., Crawley, A.M., Gee, K., Kumar, A., and Angel, J.B. (2007). IL-7 decreases IL-7 receptor α (CD127) expression and induces the shedding of CD127 by human CD8⁺ T cells. *Int. Immunol.* 19, 1329–1339.

Wherry, E.J. (2011). T cell exhaustion. *Nat. Immunol.* 12, 492–499.

Wherry, E.J., Teichgräber, V., Becker, T.C., Masopust, D., Kaech, S.M., Antia, R., von Andrian, U.H., and Ahmed, R. (2003). Lineage relationship and protective immunity of memory CD8 T cell subsets. *Nat. Immunol.* 4, 225–234.

Zanon, V., Pilipow, K., Scamardella, E., De Paoli, F., De Simone, G., Price, D.A., Martinez Usatorre, A., Romero, P., Mavilio, D., Roberto, A., et al. (2017). Curtailed T-cell activation curbs effector differentiation and generates CD8⁺ T cells with a naturally-occurring memory stem cell phenotype. *Eur. J. Immunol.* 47, 1468–1476.

Zehnder, J.L., Hirai, K., Shatsky, M., McGregor, J.L., Levitt, L.J., and Leung, L.L. (1992). The cell adhesion molecule CD31 is phosphorylated after cell activation. Down-regulation of CD31 in activated T lymphocytes. *J. Biol. Chem.* 267, 5243–5249.

iScience, Volume 23

Supplemental Information

Homeostatic Cytokines Drive Epigenetic

Reprogramming of Activated T Cells

into a “Naive-Memory” Phenotype

Guido Frumento, Kriti Verma, Wayne Croft, Andrea White, Jianmin Zuo, Zsuzsanna Nagy, Stephen Kissane, Graham Anderson, Paul Moss, and Frederick E. Chen

SUPPLEMENTAL INFORMATION

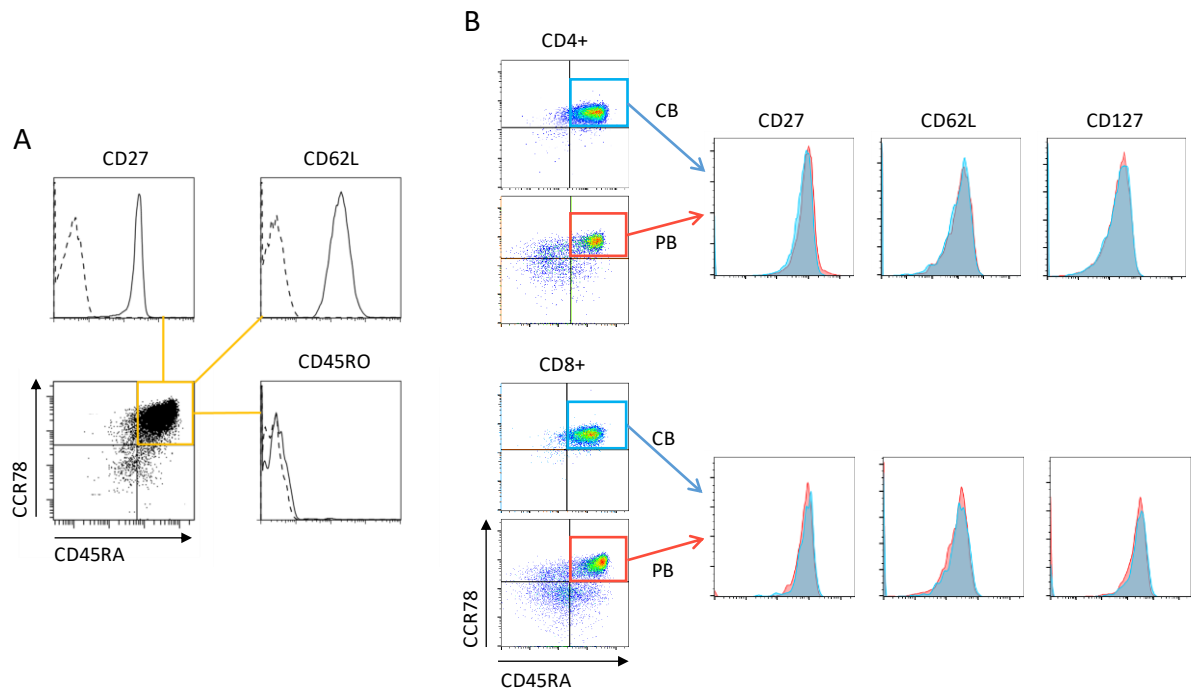


Figure S1. The basal phenotype of T_N and T_{Nrev} from CB and PB, Related to Figures 1 and 2. (A) The expression of CD27, CD45RO and CD62L in T_{Nrev} . The expression is shown for the cells having undergone phenotype reversion in Figure 1A, right panel. Dashed lines show the profiles of isotype controls. **(B)** The basal phenotype of T_N from CB and PB is shown.

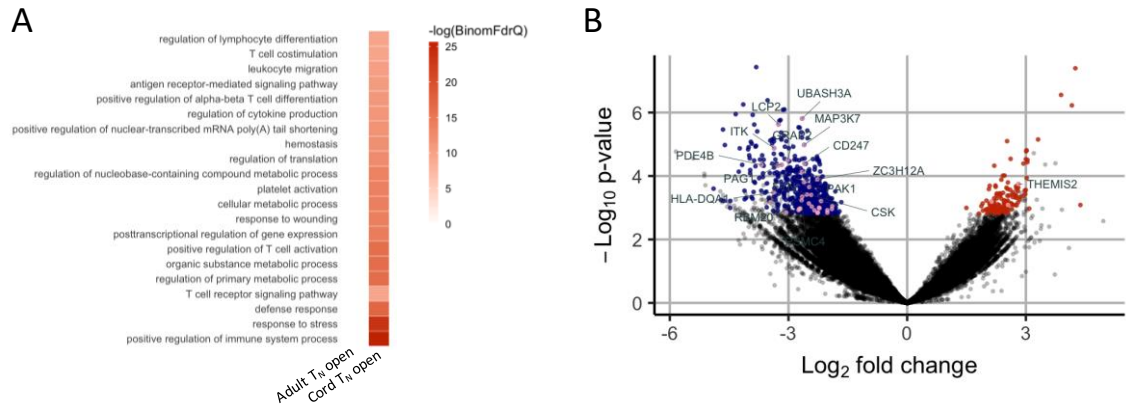


Figure S2. Pathways significantly enriched in chromatin sites preferentially open in T_N from PB or CB, Related to Figure 2. (A) Selected significant ($FDR < 0.1$) enrichments of GO terms (Biological Process) from DAC-associated gene annotations for DAC sites open in Cord T_N cells. No significant functional enrichments could be found at the sites preferentially open in samples from adults. Results are from 3 CB and 3 PB samples. (B) . Differential accessibility of peak regions identified in PB T_N cells vs CB T_N cells. The x-axis indicates Log_2 fold change and the y-axis indicates $-\text{Log}_{10}$ p-value of all peaks. Colored points indicate differentially accessible chromatin sites with inaccessible sites as blue and accessible sites as red. Points in pink are differentially accessible regions annotated as regulatory sites for genes in the biological process GO term T cell receptor signalling.

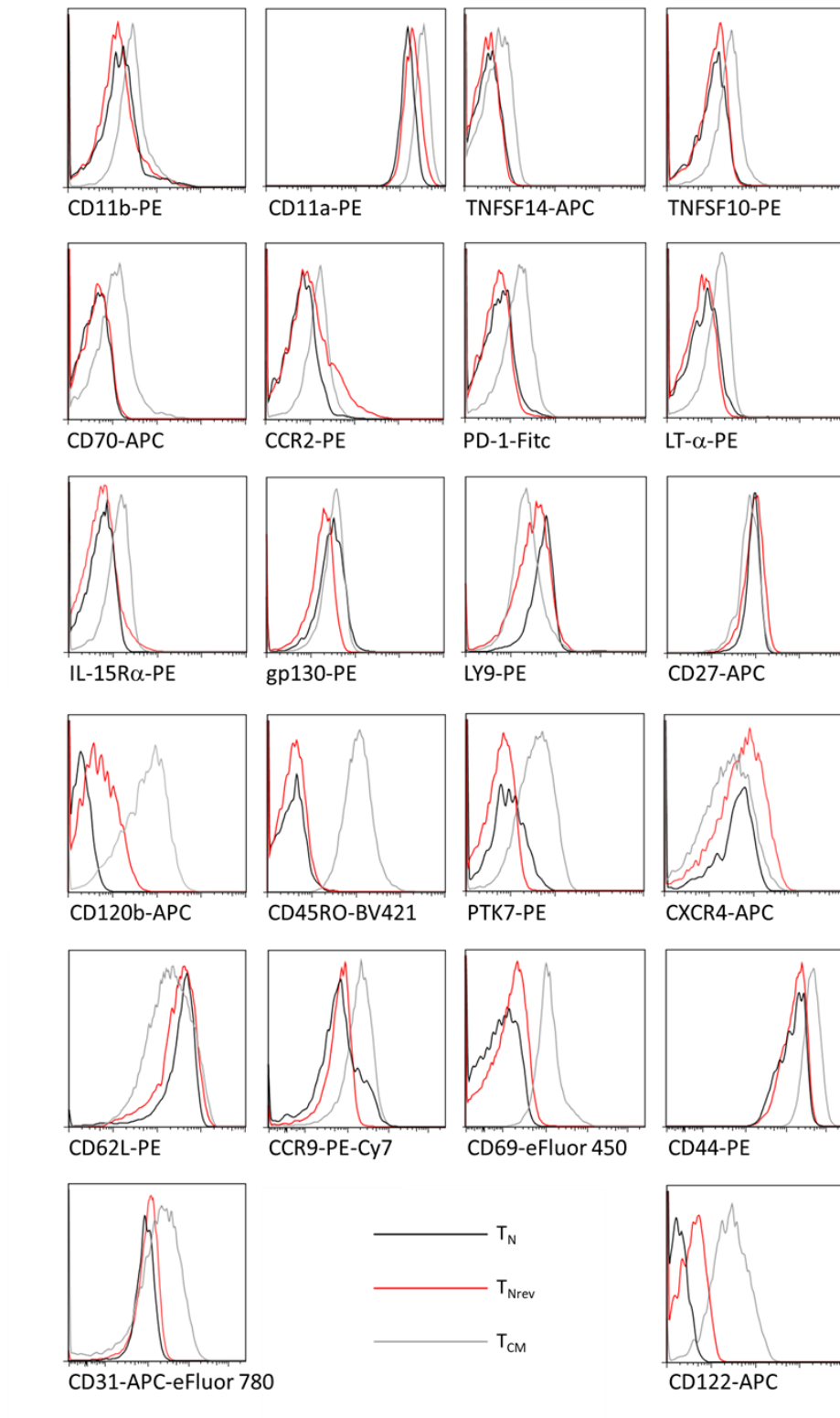


Figure S3. Extended screening for putative markers of T_{Nrev} , related to Figure 3. The membrane expression of non-discriminatory markers in T_N , recently reverted T_{Nrev} and recently differentiated T_{CM} is shown. Single representative experiment out of three.

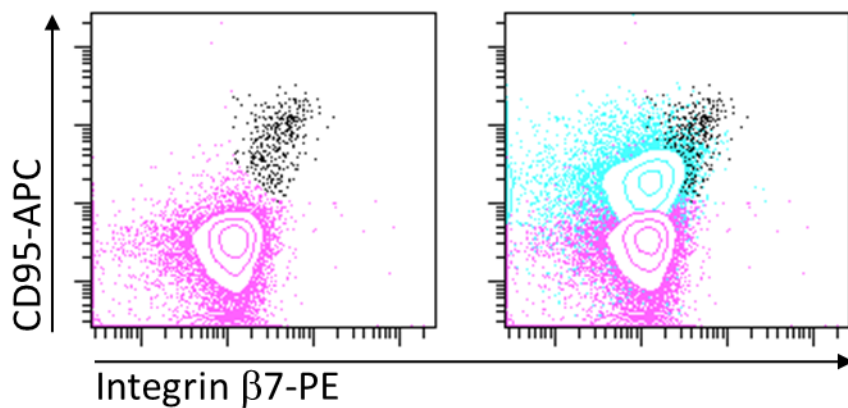


Figure S4. In tonsils, putative T_{Nrev} and memory $CD8^+$ T cells differ in the expression of CD95 and integrin $\beta 7$, Related to Figure 3. In the left panel the expression of the two markers is shown for $CCR7^+/CD45RA^+$ $CD8^+$ T cells; in the right panel the expression of CD95 and integrin $\beta 7$ in memory $CD8^+$ T cells, either $CCR7^+/CD45RA^-$, $CCR7-/CD45RA^-$ or $CCR7-/CD45RA^+$, is superimposed. In purple the classical T_N , in black the putative T_{Nrev} , and in pale blue the memory cells. Single representative experiment out of seven.

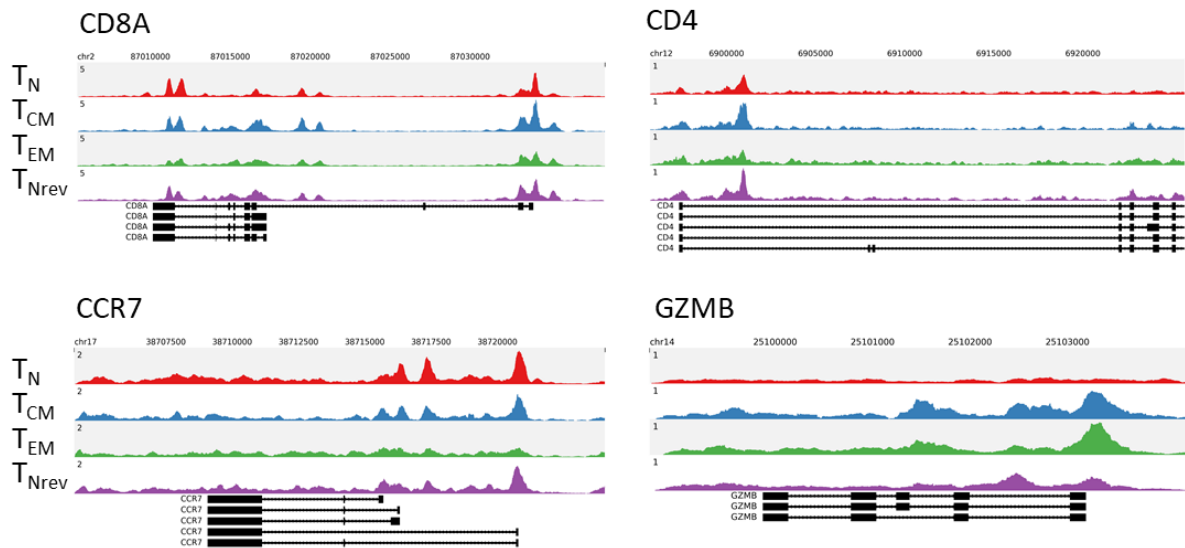


Figure S5. ATAC-seq signal tracks at selected genes confirming the purity of the samples, related to Figure 4. Gene diagrams (bottom) show alternative transcripts with black boxes indicating exons. Each subset signal is aggregated across the constituent samples, $n = 4(T_N)$, $3(T_{CM})$, $3(T_{EM})$, $4(T_{Nrev})$. The y-axes are in units of reads per million mapped reads.

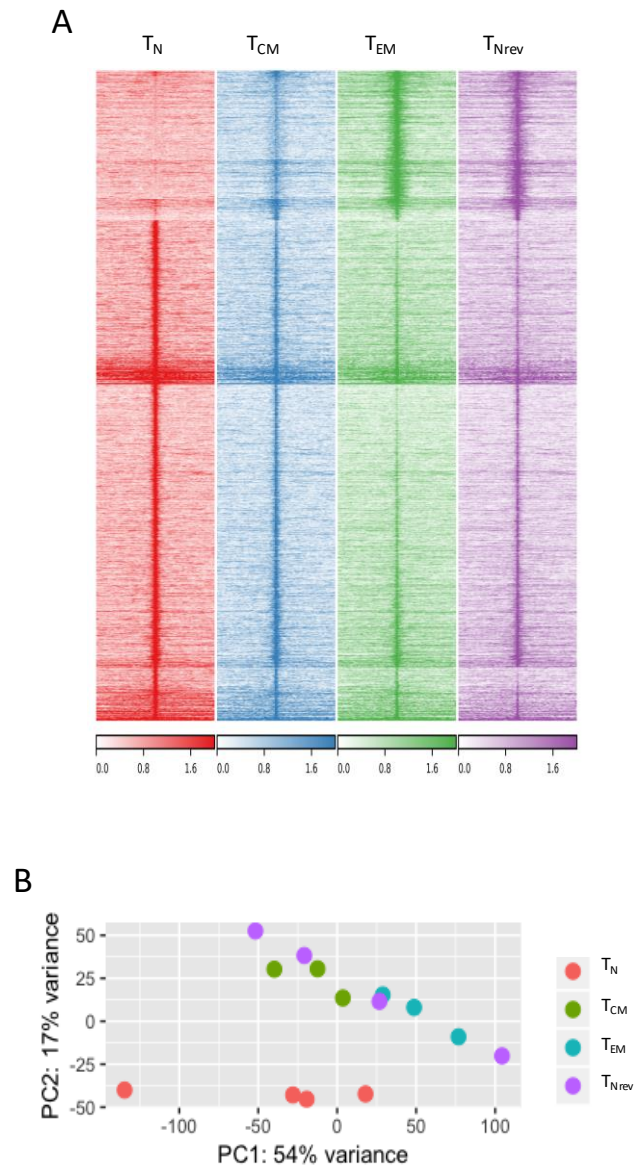


Figure S6. Comparison of chromatin landscape in T_N , T_{CM} , T_{EM} and T_{Nrev} , Related to Figure 4. (A) Peak sites that were differentially accessible in at least one pairwise comparison. Shown are normalized mapped read density (RPKM) of aggregated T_N ($n=4$), T_{CM} ($n=3$), T_{EM} ($n=3$) and T_{Nrev} ($n=4$) mapped ATAC-seq reads at differentially accessible chromatin sites (centred on peak summit, extended ± 5 kbp). (B) DACs counts for accessible and inaccessible sites are shown for T_{CM} , T_{EM} and T_{Nrev} in comparison to T_N .

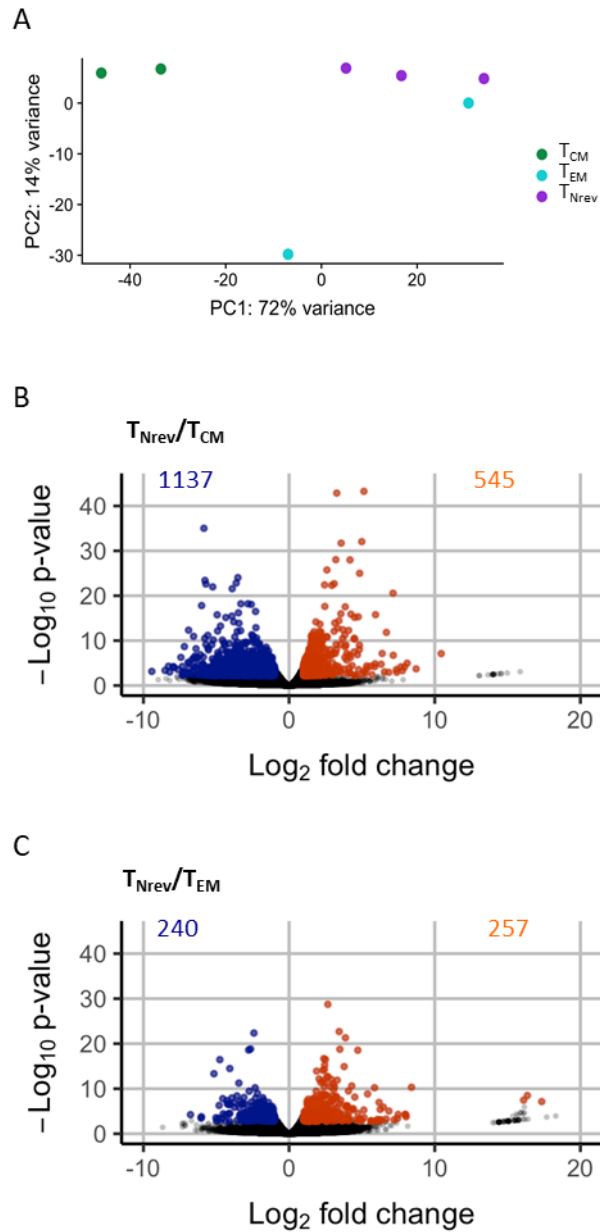
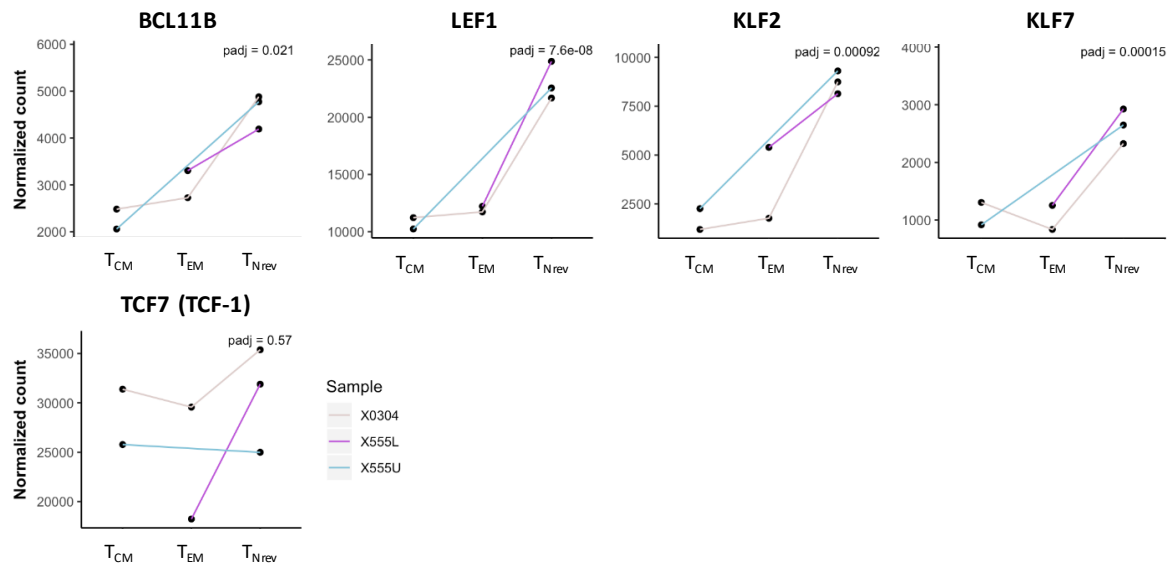


Figure S7. Transcriptomes of T_{Nrev} compared T_{Mem} cells, Related to Figure 6. Gene expression analysis was performed by RNAseq on 3 $CD8^+$ T_{Nrev} samples, and 4 $CD8^+$ T_{Mem} (2 T_{CM} and 2 T_{EM}) samples. (A) PCA plot of all samples. Pairwise comparisons of gene expression in T_{Nrev} vs T_{CM} cells (B) and T_{Nrev} vs T_{EM} (C) show $-\text{Log}_{10}$ p-value vs Log_2 fold change of all genes. Colored points indicate differentially expressed genes that are down-regulated (blue) and up-regulated (orange) in T_{Nrev} .

A



B

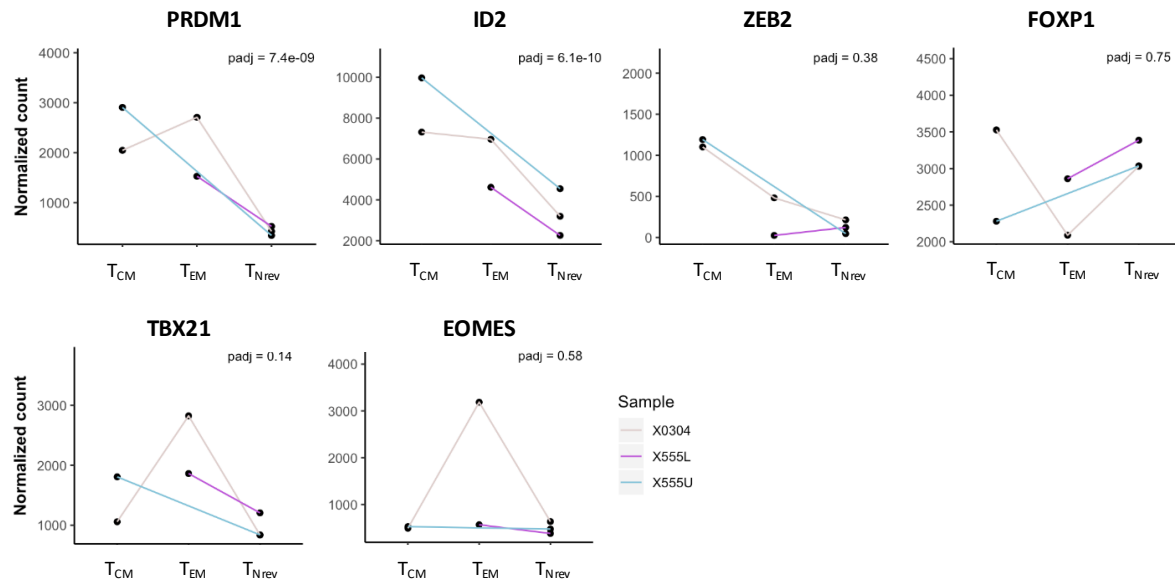


Figure S8. Stemness transcription factors of interest, Related to Figure 7. Normalized expression from RNA-seq of T_{CM}, T_{EM} and T_{Nrev} cells. Padj = p value adjusted for multiple testing from differential expression analysis of T_{Nrev} vs T_{CM} and T_{EM} cells. Key Transcription factors with known increased (A) and decreased (B) expression.

Table S1. Cell numbers are not altered by phenotypic reversion, Related to Figure 1.

	CB 1		CB 2		CB 3	
	Day6	Day 16	Day8	Day 18	Day6	Day 20
CCR7 ⁺ /CD45RA ⁺	32,1 ^A	872,1	9	345,5	21,3	1769,3
CCR7 ⁺ /CD45RA ⁻	982,2	256,6	782,2	303,2	1560,9	487,9
CCR7 ⁻ /CD45RA ⁻	308	79,2	183,7	101,4	213,2	33,1
CCR7 ⁻ /CD45RA ⁺	5,4	72	1,4	32	2,9	43
Total	1327,7	1279,9	976,3	782,1	1798,3	2333,3

^A Absolute number of CD8⁺ T cells within different subsets at T_N nadir (days 6 and 8) and T_{Nrev} plateau (days 16, 18 and 20). Cell counts (x10³) from 3 different CB samples, enumerated using Trucount beads.

Table S2. GREAT analysis, Related to Figure 5.

216 TNrev accessible sites			
		NO ENRICHMENT	
401 TNrev and TEM accessible sites			
		NO ENRICHMENT	
890 TEM accessible sites			
		NO ENRICHMENT	
546 TNrev inaccessible sites			
	Binom Rank	Binom Raw P-Value	Binom FDR Q-Val
Signaling events mediated by focal adhesion kinase	2	2.16441E-06	0.001428513
Signaling events mediated by Hepatocyte GF Receptor (c-Met)	3	2.50412E-06	0.001101811
T Cytotoxic Cell Surface Molecules	5	1.64991E-05	0.004355768
Keratinocyte Differentiation	7	0.000126032	0.023766053
PDGFR-beta signaling pathway	10	0.000228715	0.03019034
HIF-1-alpha transcription factor network	15	0.000471389	0.041482267
1648 TNrev and TEM inaccessible sites			
	Binom Rank	Binom Raw P-Value	Binom FDR Q-Val
TCR signaling in naive CD4+ T cells	1	2.46E-27	3.24E-24
Genes involved in Immune System	2	3.81E-26	2.51E-23
TCR signaling in naive CD8+ T cells	3	1.18E-22	5.18E-20
T cell receptor signaling pathway	4	4.57E-21	1.51E-18
Thromboxane A2 receptor signaling	5	2.33E-18	6.14E-16
Genes involved in Generation of second messenger molecules	6	3.36E-17	7.40E-15
Keratinocyte Differentiation	7	5.08E-17	9.58E-15
CXCR4-mediated signaling events	8	7.31E-17	1.21E-14
Genes involved in TCR signaling	9	2.35E-15	3.44E-13
Genes involved in Adaptive Immune System	10	2.23E-14	2.94E-12
T Cell Signal Transduction	11	7.59E-14	9.10E-12
Genes involved in Platelet activation, signaling and aggregation	12	5.48E-13	6.03E-11
HIF-1-alpha transcription factor network	13	2.49E-11	2.53E-09
Signaling events mediated by VEGFR1 and VEGFR2	14	5.20E-11	4.90E-09
Genes involved in Cytokine Signaling in Immune system	15	1.64E-10	1.44E-08
Signaling events mediated by focal adhesion kinase	16	2.42E-10	2.00E-08
Genes involved in Lipoprotein metabolism	17	3.53E-10	2.74E-08
Role of Calcineurin-dependent NFAT signaling in lymphocytes	19	7.14E-10	4.96E-08
Genes involved in Lipid digestion, mobilization, and transport	21	7.27E-10	4.57E-08
Genes involved in Signaling by NOTCH	22	9.66E-10	5.80E-08
2868 TEM inaccessible sites			
	Binom Rank	Binom Raw P-Value	Binom FDR Q-Val
Genes involved in Adaptive Immune System	2	1.11E-23	7.36E-21
TCR signaling in naive CD4+ T cells	3	1.88E-23	8.28E-21
TCR signaling in naive CD8+ T cells	4	1.89E-21	6.24E-19
T cell receptor signaling pathway	5	9.77E-20	2.58E-17
CXCR4-mediated signaling events	6	8.47E-19	1.86E-16
Class I PI3K signaling events	7	1.36E-17	2.57E-15
Genes involved in TCR signaling	8	8.07E-16	1.33E-13
Natural killer cell mediated cytotoxicity	9	4.53E-15	6.64E-13
Genes involved in Cytokine Signaling in Immune system	10	8.55E-15	1.13E-12
T Cell Receptor Signaling Pathway	11	7.90E-14	9.48E-12
Genes involved in Signaling by the B Cell Receptor (BCR)	12	8.12E-14	8.94E-12
Genes involved in Phosphorylation of CD3 and TCR zeta chains	13	6.23E-13	6.33E-11
IL2-mediated signaling events	15	2.12E-12	1.86E-10
Signaling events mediated by focal adhesion kinase	16	3.08E-12	2.54E-10
Lck and Fyn tyrosine kinases in initiation of TCR Activation	17	6.43E-12	4.99E-10
PDGFR-beta signaling pathway	18	6.77E-12	4.97E-10
IL-7 Signal Transduction	19	3.86E-11	2.68E-09
Downstream signaling in naive CD8+ T cells	20	4.83E-11	3.19E-09
Thromboxane A2 receptor signaling	21	9.06E-11	5.69E-09
Fc-epsilon receptor I signaling in mast cells	22	1.15E-10	6.87E-09

Table S5. List of the antibodies used for flow cytometry, Related to Figure 1, Figure 2, Figure 3, Figure 5.

Antigen/ fluorochrome	Clone	Purchased from	Antigen/ fluorochrome	Clone	Purchased from
CCR2/PE	K036C2	BioLegend	CD45RA/Fitc	HI100	BD
CCR7/Fitc	G043H7	BD	CD45RA/PE-Cy7	HI100	BD
CCR7/PE	G043H7	R&D	CD45RO/BV421	UCHL1	BioLegend
CCR7/BV605	G043H7	BioLegend	CD49d/PE	9F10	eBioscience
CCR9/PE-Cy7	L053E8	BioLegend	CD62L/PE	DREG-56	BD
CD11a/PE	HI111	BD	CD69/eFluor 450	FN50	eBioscience
CD11b/PE	ICRF44	BD	CD70/APC	113-16	BioLegend
CD120b/APC	22235	R&D	CD8/Fitc	SK1	BD
CD122/APC	TU27	BioLegend	CD8/Pacific Blue	RPA-T8	BD
CD127/PE	A019D5	BioLegend	CD95/APC	DX2	BD
CD14/Pacific Blue	TuK4	Invitrogen	CXCR3/APC	1C6/CXCR3	BD
CD14/PerCP	134620	R&D	CXCR4/APC	12G5	eBioscience
CD16/Pacific Blue	3G8	Invitrogen	gp130/PE	28126	R&D
CD16/PerCP	245536	R&D	granzyme B/Fitc	GB11	BD
CD19/Pacific Blue	SJ25-C1	Invitrogen	IL-15Ra/PE	JM7A4	BioLegend
CD19/PerCP	4G7-2E3	R&D	Integrin β 7/PE	473207	R&D
CD25/APC-Cy7	M-A251	BD	LT- α /PE	359-81-11	BioLegend
CD27/APC	57703	R&D	LY-9/PE	hLY-9.1.25	BioLegend
CD3/PE	OKT3	BioLegend	PD-1/Fitc	MIH4	BD
CD3/V500	UCHT1	BD	Perforin/Fitc	Dg9	eBioscience
CD31/APC-eFluor 780	WM-59	eBioscience	PTK7/PE	188B	Miltenyi
CD4/Fitc	SK3	eBioscience	TNFSF10/PE	RIK-2	BioLegend
CD44/PE	BJ18	BioLegend	TNFSF14/APC	115520	R&D

TRANSPARENT METHODS

Cell separation and culture.

The study was approved by the National Research Ethics Committee, UK REC no. 11/WM/0315, and by the Non-Clinical Issue committee of the NHS Blood and Transplant. Human CB from anonymized collections unsuitable for banking, was provided by the NHS Cord Blood Bank, UK, as Non-Clinical Issue. Peripheral blood (PB) was collected from consenting adult healthy blood donors from the NHS Blood and Transplant Donor Centre, Birmingham, UK.

PB mononuclear cells (PBMCs) and CBMCs were obtained by Ficoll separation. CD8⁺ T_N and T_{Nrev} were enriched using the Naïve CD8⁺ T cell Isolation Kit (Miltenyi Biotech, Bergisch Gladbach, Germany). CD8⁺ T_{EM} cells were negatively isolated after activation of enriched CD8⁺ T_N by removal of CCR7⁺ and CD45RA⁺ cells with anti-CCR7-APC, anti-CD45RA-APC and anti-APC MicroBeads (Miltenyi). CD8⁺ T_{CM} cells were isolated from less differentiated samples by depletion of CD45RA⁺ cells with anti CD45RA-APC and anti-APC MicroBeads. Cells were cultured in RPMI 1640 plus 10% FCS. CD4⁺ T_N cells were isolated with the Naïve CD4⁺ T cell Isolation Cell Isolation Kit II (Miltenyi).

CD8⁺ T_{CM/EM} cells were negatively isolated from CD8⁺ T_N cells isolated as indicated above by removal of CD45RA⁺ cells with anti-CD45RA-APC and anti-APC MicroBeads (Miltenyi).

Dendritic cells (DCs) were generated from adherent mononuclear cells after incubating in plates for 2 hours. Adherent cells were cultured in the medium supplemented on days 0, 3 and 6 with 50 ng/ml GM-CSF and 500 U/ml IL-4. On day 6, DCs were matured by adding 2 ng/ml IL-1 β , 1000 U/ml IL-6 and 10 ng/ml TNF α (all from R&D Systems, Minneapolis, USA) (1997). DCs were recovered after a further 48 hours.

Mononuclear cells from tonsils were kindly provided by P Murray and E Nagy. Tonsils were obtained after tonsillectomy for recurrent acute tonsillitis, minced and dissociated by mechanical means and mononuclear cells were collected by Ficoll separation.

TCR gene transduction.

CBMCs were retrovirally transduced with a TCR, specific for the HLA A11-restricted SSCSSCPLSK (SSC) peptide of the LMP2 protein of Epstein Barr virus, as previously described (Frumento *et al*, 2013). Briefly, cells were transduced with retrovirus 48 hours after activation. The retrovirus used was the pMP71-PRE vector (provided by C. Baum, Hannover, Germany) with genes encoding TCR α and β chains isolated from an EBV-specific CD8⁺ T cell clone that targets the HLA A*1101-restricted epitope SSC derived from the viral protein LMP2 (Zheng *et al.*, 2015). To generate the retrovirus, Phoenix amphotropic packaging cells were transfected with the pMP71-PRE vector using FuGENE HD (Roche, Basel, Switzerland). After 48 hours the retroviral supernatant was recovered. Preactivated cells were seeded at 4–6 × 10⁶ cells/well in 1 ml RPMI onto 6-well plates coated with retronectin (Takara, Shiga, Japan). Retroviral supernatant (1.5 ml/well) or medium alone (mock-transduced) was added to each well and centrifuged for 1 h × 800 g at 30°C. Also described are generation of DCs, their loading with the peptide, and re-stimulation of transduced T cells with peptide-pulsed DCs.

Cell activation and treatment.

Cells were activated, or re-activated, with either of the following stimuli.

Anti-CD3: cells were incubated with 66 ng/ml anti-CD3 antibody (OKT3), plus 300 U/ml IL-2 (Miltenyi).

Anti-CD3 and crosslinked anti-CD28: cells were incubated with 66 ng/ml OKT3 plus a mix of 66 ng/ml LEAF anti-CD28 (BioLegend, San Diego, CA, USA) and 66 ng/ml rat anti-mouse IgG1 (BioLegend), and 50 U/ml IL-2.

CD3/CD28 beads: Dynabeads T Activator CD3/CD28 (Life Technologies, Grand Island, NY)

beads were incubated with CBMCs at 1:1 ratio in the presence of 30 U/ml IL-2.

PHA: cells were incubated with 1% PHA M (Life Technologies, Carlsbad, CA, USA), plus 50 U/ml IL-2.

SEB: cells were incubated with 1 µg/ml SEB (Sigma-Aldrich, St. Louis, MO, USA), plus 50 U/ml IL-2.

From day 2, IL-2 100 U/ml, for stimulation with soluble anti-CD3, or 30 U/ml, for the other cases, was added thrice a week.

Phenotype was checked thrice a week. When the percentage of CCR7⁺/CD45RA⁺ CD8⁺ T cells dropped

below 20%, half of the medium was replaced with fresh medium containing either IL-2, IL-4, IL-6, IL-7,

IL-15 or IL-21 (all from Miltenyi), or combinations thereof, at final concentrations of 30 U/ml, 25 ng/ml,

10 ng/ml, 25 ng/ml, 50 ng/ml, and 50 ng/ml, respectively. Thrice a week, half of the culture medium was replaced with new medium plus cytokine(s). Re-activation by phorbol myristate acetate (PMA) plus ionomycin (Cell Stimulation Cocktail, eBioscience, San Diego, CA, USA) was performed exactly following manufacturer's instructions. BMS 493 (Tocris, Bristol, UK) was preincubated 3 hours before addition of IL_7 and/or all-trans-retinoic acid (ATRA, Sigma Aldrich).

Flow cytometry.

The antibodies used for cell membrane staining are listed in Table S5. Gating strategy involved selection of single cells and use of a "dump channel" including either 7-aminoactinomycin D (BD, San Jose, CA, USA) and PerCP-conjugated anti CD14, CD16 and CD19, or Live/Dead Fixable Violet (Thermo Fisher Scientific, Wilmington, DE, USA) and Pacific Blue-conjugated anti CD14, CD16 and CD19. Proliferation was evaluated by staining cells with 1 μ M CFSE. For intracellular staining, cells were fixed and permeabilized using the FIX&PERM kit (ADG, Kaumberg, Austria) or Fixation/Permeabilization Solution Kit (BD) for staining of cytokines or TFs, respectively. Indirect staining was carried out for E2F-1 (clone 8G9, Novus Biologicals, Littleton, CO, USA) and KAT2B (clone EPR2670, Abcam, Cambridge, MA, USA). In this case a PE- conjugated rat anti-mouse IgG1 (clone RMG1-1, BioLegend, San Diego, CA, USA) and an APC-conjugated goat ant-rabbit IgG (R&D, Minneapolis, MN, USA) were used, respectively. In some experiments cells were enumerated using Trucount Beads (BD). Transduced lymphocytes were identified using HLA A*1101:SSC peptide-specific pentamers and Tag/PE (Proimmune, Oxford, UK). Flow cytometry was performed on either a FACSCanto II, an LSR II, or a Fortessa (BD) flow cytometer. Quantifications were made on the basis of FACSDiva and FlowJo (both from BD) softwares.

Cytotoxicity assay.

Cytotoxicity of transduced T cells was assessed in a standard ^{51}Cr assay. Briefly, HLA A*1101-transduced T2 cells were loaded with the concentrations of SSC peptide indicated in the text, then used as targets at 2500 cells/well in a 5 hrs test.

ATAC-seq library preparation and analysis

For sequencing the open chromatin regions in the CD8⁺ T cell subsets, we used a previously published method with slight modification (Brignall *et al*, 2017). In brief, 50,000 cells were sorted on a cell sorter (FACSARIA, BD) and pelleted by centrifugation at 500 × *g* and 4°C for 10 min. The cell pellet was washed once with cold PBS and centrifuged again. Pellets were resuspended in a 50-μl reaction cocktail containing 1 μl of 0.5% Digitonin (Promega, Madison, WI, USA), 2.5 μl of Tn5 transposase and 25 μl of TD buffer (Nextera DNA library preparation kit, Illumina, San Diego, CA, USA) and incubated for 30 min at 37°C with gentle shaking. The tagmented DNA was then purified using Minielute PCR Purification kit (Qiagen, Hilden, Germany) and eluted into 11 μl of elution buffer. The transposed DNA was then amplified using 2.5 μl of indexing primers and 25 μl of Nextera PCR master mix according to the PCR protocol previously described (Buenrostro *et al*, 2013). PCR clean-up was then performed using AMPure XP beads (Beckman Coulter, Brea, CA, USA), and resuspended in 30 μl of resuspension buffer. The libraries were quantified using Qubit fluorometer (Life Technologies), and the size was determined using TapeStation (Agilent, Santa Clara, CA, USA). Sequencing was performed on a High Throughput Benchtop NextSeq 500/550 Sequencer using NextSeq[®] 500/550 High Output Kit v2 - 75 cycles (Illumina, San Diego, CA, USA).

ATAC-seq data was aligned to the human genome (hg19) using Bowtie2 v2.2.9 with the settings: `--very-sensitive-local` (Langmead and Salzberg, 2012). Peaks were called on the alignments using MACS2 v2.2 with settings: `--keep-dup=auto --nomodel --shift -100 --extsize 200` (Zang *et al*, 2008). Peaks were annotated with closest gene (by RefSeq transcription start site) and average tag counts (400bp region centred on peak summit) using `annotatePeaks` from HOMER v4.8. Motif enrichment at peak regions was assessed using the HOMER program `findMotifsGenome` (Heinz *et al*, 2010). DACs were identified by pairwise comparisons in the R package DESeq2 (Love *et al*, 2014). Genome-wide average profile data at TSS and enhancer sites was obtained using `ngs.plot` v2.63 (Shen *et al*, 2014). Heatmaps of DACs and mapped read profiles at selected genomic regions were obtained using `fluff` v2.1.4 (Georgiou *et al*,

2016). ATAC-seq data have been deposited in Gene Expression Omnibus, accession number GSE120618, public release December 2018.

Microarray analysis.

Gene expression analysis was performed on 3 CD8⁺ T_{Nrev} at day 19 and 3 CD8⁺ T_N samples. RNA extraction was performed using RNeasy columns (Qiagen). Source RNA was confirmed as high quality by use of a Bioanalyzer 2100 (Agilent). RNA Integrity Numbers of 6.0 were confirmed for all samples using a RNA 6000 Pico Chip kit (Agilent). 25ng of each source sample RNA was labeled with Cy3 dye using the Low Input Quick Amp Labelling Kit (Agilent). A specific activity of greater than 6.0 was confirmed by measurement with a spectrophotometer. 600 ng of labeled RNA was hybridized to SurePrint G3 Human 8x60K microarray slides (Agilent). After hybridization, slides were scanned with a High Resolution C Scanner (Agilent), using a scan resolution of 3 mm. Feature extraction was performed using Feature Extraction Software (Agilent), with no background subtraction. Extracted data were normalized using the R 3.4 software environment with the limma 3.32.5 analysis package (Smyth, 2004). Log transformed expression values were analyzed in limma using a moderated paired t-test. Microarray data that support the findings of this study have been deposited in Gene Expression Omnibus, accession number GSE114812, public release December 2018.

RNA-seq analysis

RNA extraction was performed using RNeasy columns (Qiagen). TruSeq mRNA library preparation and sequencing was carried out by Edinburgh Genomics, The University of Edinburgh. Sequencing data were generated using NovaSeq 50PE.

Statistics

Quantifications of events from flow cytometry were made using FACSDiva and FlowJo (both from BD) softwares.

Genes were classified as differentially expressed if Benjamini-Hochberg adjusted p-value <0.05 and absolute fold change >2. Peaks discovered from the ATAC-seq analysis were classified as differentially

accessible in a given pairwise comparison if **Benjamini-Hochberg adjusted p-value <0.1 and absolute log₂ fold change >1**. Pathway enrichment analysis was performed using G:profiler (Reimand *et al*, 2016) with a threshold adjusted p-value of <0.05 for reporting significant enrichments. Gene-set enrichment analysis (GSEA) was performed using the Bioconductor R package GAGE (Luo *et al*, 2009). The Hallmark and Canonical Pathways gene sets were downloaded from Molecular Signatures Database (MSigDB) (Liberzon *et al*, 2015). GSEA was also used to assess enrichment of published gene signatures for T_{SCM} up/down-regulated vs T_N (Gattinoni *et al*, 2011) and T_{MNP} up/down-regulated vs T_N (Pulko *et al*, 2016). T_{MNP} up/down-regulated genes vs T_N were extracted from published RNAseq count data downloaded from NCBI's Gene Expression Omnibus (GSE80306). Differentially expressed genes (DEGs) with Benjamini-Hochberg adjusted p-value<0.05 and absolute fold change >2 were identified using the R package DEseq2. Genomic Regions Enrichment of Annotations Tools (GREAT) (McLean *et al*, 2010) was used to identify functional enrichments within genes annotated as closest to differentially accessible chromatin sites. Functional and network analysis was performed on the pool of significant genes using Ingenuity Pathway Analysis (Qiagen).

In all the other cases statistical analysis was carried out using Graph Pad Prism software or Excel 2016. Results in graphs are reported as mean ± 1SD.

SUPPLEMENTAL REFERENCES

Brignall R, Cauchy P, Bevington SL, Gorman B, Pisco AO, Bagnall J, Boddington C, Rowe W, England H, Rich K et al (2017). Integration of kinase and calcium signaling at the level of chromatin underlies inducible gene activation in T cells. *J. Immunol.* 199, 2652-2667.

Buenrostro JD, Giresi PG, Zaba LC, Chang HY, Greenleaf WJ (2013). Transposition of native chromatin for fast and sensitive epigenomic profiling of open chromatin, DNA-binding proteins and nucleosome position. *Nat. Methods* 10, 1213-1218.

Georgiou G, van Heeringen SJ (2016). fluff: exploratory analysis and visualization of high-throughput sequencing data. *PeerJ* 19, e2209.

Heinz S, Benner C, Spann N, Bertolino E, Lin YC, Laslo P, Cheng JX, Murre C, Singh H, Glass CK (2010). Simple combinations of lineage-determining transcription factors prime cis-regulatory elements required for macrophage and B cell identities. *Mol. Cell* 38, 576-589.

Langmead B, Salzberg S (2012). [Fast gapped-read alignment with Bowtie 2](#). *Nat. Methods* 9, 357-359.

Liberzon A, Birger C, Thorvaldsdóttir H, Ghandi M, Mesiro, JP, Tamayo P (2015). The Molecular Signatures Database (MSigDB) hallmark gene set collection. *Cell Syst.* 1, 417-425.

Love MI, Huber W, Anders S (2014). Moderated estimation of fold change and dispersion for RNA-seq data with DESeq2. *Genome Biol.* 15, 550.

Luo W, Friedman MS, Shedden K, Hankenson KD, Woolf PJ (2009). GAGE: generally applicable gene set enrichment for pathway analysis. *BMC Bioinformatics* 10, 161.

McLean CY, Bristor D, Hiller M, Clarke SL, Schaar BT, Lowe CB, Wenger AM, Bejerano G (2010). GREAT improves functional interpretation of cis-regulatory regions. *Nat. Biotechnol.* 28, 495-501.

Reimand J, Arak T, Adler P, Kolberg L, Reisberg S, Peterson H, Vilo J (2016). g:Profiler-a web server for functional interpretation of gene lists. *Nucleic Acids Res.* 44, W83-89.

Shen L, Shao N, Liu X, Nestler E (2014). ngs.plot: Quick mining and visualization of next-generation sequencing data by integrating genomic databases. *BMC Genomics* 15, 284.

Zhang Y, Liu T, Meyer CA, Eeckhoutte J, Johnson DS, Bernstein BE, Nusbaum C, Myers RM, Brown M, Li W et al (2008). Model-based analysis of ChIP-Seq (MACS). *Genome Biol.* 9, R137.

Zheng Y, Parsonage G, Zhuang X, Machado LR, James CH, Salman A, Searle PF, Hui EP, Chan AT, Lee SP (2015). Human Leukocyte Antigen (HLA) A*1101-Restricted Epstein-Barr Virus-Specific T-cell Receptor Gene Transfer to Target Nasopharyngeal Carcinoma. *Cancer Immunol. Res.* 3, 1138-1147.